Thesis for the Degree of Doctor of Philosophy

Large eddy simulation of combustion using linear-eddy subgrid modeling

Salman Arshad

Department of Mechanics and Maritime Sciences
Chalmers University of Technology
Göteborg, Sweden 2019

Large eddy simulation of combustion using linear-eddy subgrid modeling
Salman Arshad
ISBN 978-91-7597-882-6

Doktorsavhandlingar vid Chalmers tekniska högskola
Ny serie nr 4563
ISSN 0346-718X

Department of Mechanics and Maritime Sciences
Chalmers University of Technology
SE–412 96 Göteborg
Sweden
Telephone: +46 (0)31 – 772 1000

Typeset by the author using LaTeX.

Chalmers Reproservice
Göteborg, Sweden 2019

Abstract

As emissions regulations are getting stricter and efficiency requirements of internal combustion engines (ICE) are increasing, different concepts to improve combustion are being investigated. For example lean stratified premixed combustion, homogeneous charge compression ignition (HCCI), use of more exhaust gas recirculation (EGR) to reduce NOx etc. In all these concepts, combustion happens at lower temperatures, higher pressures, and higher level of air dilution than today's typical spark ignition or diesel engines.

Many combustion models in computational fluid dynamics (CFD) today describe either premixed or non-premixed mode of combustion, assuming fast chemistry regimes only. There is a great need for new combustion models that are mode (premixed/non-premixed) and regime (fast/non fast chemistry) independent. The linear-eddy model (LEM) of Kerstein [1] used as a subgrid combustion model for large eddy simulation (LES) called LES-LEM is regarded as a truly mode and regime independent combustion model as it models all the physical processes, i.e. large and small scale turbulent advection, molecular diffusion and chemical reactions at their respective length and time scales.

In this dissertation, a new LEM closure for LES-LEM using the reaction-rate approach is proposed in which the LEM provides closure for the chemical source terms in the conservation equations of the sensible enthalpy and species mass. The new LEM closure is tested on a bluff-body premixed flame problem and simulation results are compared with experiments.

Furthermore, a new splicing approach for modeling large-scale advection in LES-LEM is presented. The approach links the subgrid LEM implementation to a concept of control-volume crossing rate. A dedicated investigation of splicing is done by simulating passive scalar mixing without the complexity of chemically reacting flow physics.

Lastly, an improved modeling technique called super-grid LES-LEM is proposed to computationally speed-up LES-LEM.

List of publications

This thesis is based on the following appended papers:

Paper 1

E.D. Gonzalez-Juez, A. Dasgupta, S. Arshad, M. Oevermann, D. Lignell, "Effect of the turbulence modeling in large-eddy simulations of nonpremixed flames undergoing extinction and reignition", *55th AIAA Aerospace Sciences Meeting, AIAA SciTech Forum, AIAA 2017-0604*, Grapevine, TX (2017).

Paper 2

E.D. Gonzalez-Juez, S. Arshad, M. Oevermann, S. Menon, "Turbulent-combustion closure for the chemical source terms using the linear-eddy model", *53rd AIAA/SAE/ASEE Joint Propulsion Conference, AIAA Propulsion and Energy Forum, AIAA 2017-5080*, Atlanta, GA (2017).

Paper 3

S. Arshad, B. Kong, A.R. Kerstein, M. Oevermann, "A strategy for large-scale scalar advection in large eddy simulations that use the linear eddy sub-grid mixing model", *International Journal of Numerical Methods for Heat and Fluid Flow, Vol. 28 Issue: 10, pp.2463-2479* (2018).

Paper 4

S. Arshad, E.D. Gonzalez-Juez, A. Dasgupta, S. Menon, M. Oevermann, "Subgrid reaction-diffusion closure for large eddy simulations using the linear-eddy model", *Flow, Turbulence and Combustion*, In press.

Acknowledgments

First of all, I would like to express my special thanks to my supervisor Professor Michael Oevermann for his guidance, great support, all the fruitful discussions and patience. My warm thanks goes to Alan Kerstein for all the great ideas and explanations. I am thankful to Esteban D. Gonzalez-Juez and Adhiraj Dasgupta for excellent cooperation as working together with them was a great pleasure.

Thanks to Professor Ingemar Denbratt for giving me the chance to work on this interesting PhD project at the division of combustion and propulsion systems.

I would like to thank the Swedish Research Council and Combustion Engine Research Center (CERC) for financial support of the project. In addition, thanks to the Swedish National Infrastructure for Computing (SNIC) at C3SE Chalmers for providing resources for the simulations.

Thanks to all my colleagues in the combustion and propulsion systems division. Moreover I would like to thank my friends in Sweden for fun times.

Finally, I would thank from the bottom of my heart to my whole family. Thanks for all the support throughout my life.

Contents

Abstract **i**

List of publications **iii**

Acknowledgments **v**

Contents **vii**

Introduction **1**

1 Model formulation **9**
1.1 Introduction 10
1.2 LES equations 10
1.3 LEM subgrid modeling inside a LES cell 11
1.4 Large-scale advection modeling 14
1.4.1 New splicing algorithm 16
1.4.2 Parallel splicing 18
1.4.3 Splicing at inlet and outlet boundaries 19
1.5 Closure of the chemical source terms with LEM 19

2 Model validation **23**
2.1 Introduction 24
2.2 Combustion simulations 24
2.2.1 Comparison with experiments and WSR model . . . 25
2.2.2 Comparison with traditional LES-LEM 28
2.3 Splicing investigation 31
2.3.1 Comparisons with experiments 32
2.3.2 Comparison of the new and old splicing strategy . . . 33

Conclusion **35**

Future work **37**

Summary of papers **41**

References **43**

Paper 1
Effect of the turbulence modeling in large-eddy simulations of non-premixed flames undergoing extinction and reignition 54

Paper 2
Turbulent-combustion closure for the chemical source terms using the linear-eddy model 72

Paper 3
A strategy for large-scale scalar advection in large eddy simulations that use the linear eddy subgrid mixing model 92

Paper 4
Subgrid reaction-diffusion closure for large eddy simulations using the linear-eddy model 112

Introduction

Combustion has been used by humans for thousands of years for practical purposes of cooking food and heating homes. With the advent of the steam engine, a new use of combustion was found, i.e. to produce work. Steam engines were used particularly in railroads and steam ships. After the discovery of gasoline, steam engines were replaced with internal combustion engines (ICE), which are still being used extensively for e.g. transportation and power generation purposes. However, tremendous use of ICE has lead to various environmental and health hazards. So modern research on combustion in ICE has two major objectives, i.e. the optimization of combustion efficiency and the reduction of pollutants. In order to achieve these objectives, a clear understanding of the processes taking place during combustion is a prerequisite. This understanding will only be obtained by a joint approach of experiments and modeling.

Turbulent combustion happening in ICE involves an interaction between highly non-linear chemical reactions, turbulence and molecular mixing. Turbulence is characterized by a broad range of scales in spacetime, ranging from the smallest Kolmogorov scales to the largest flow structures characterized by the scales of the geometry. Computational fluid dynamics (CFD) provides useful tools to study turbulent combustion. In CFD, the governing equations are numerically solved. The computational domain is divided into a finite number of cells on which the governing equations are discretized and then solved. Direct numerical simulation (DNS) is a CFD tool which aims at fully resolving the flow physics. However, DNS is currently computationally affordable only for relatively simple problems and thus non-feasible for practical flow problems (such as ICE). In contrast, CFD approaches for engineering problems approximate the flow physics with mathematical formulations called turbulent combustion models. There are numerous turbulent combustion models available [2,3] and several studies have compared them, see [4–6] for a few examples.

Large eddy simulation (LES) is a popular modeling approach for simulating turbulent combustion. LES resolves the energy containing large-scale turbulent motion directly and models the effect of unresolved small scales,

resulting in lower grid resolution requirements compared to DNS. For scalar mixing, LES has shown better predictive capabilities than Reynolds Averaged Navier Stokes (RANS) approaches [7]. Fig. 1 shows portion of the energy spectrum resolved by RANS, LES and DNS respectively. In LES, large scales of the flow are separated from the smaller scales of the flow by applying a spatial filter on the governing equations. LES has shown a good predictive capability in many studies related to ICE. Just a few examples include work done by Jhavar and Rutland [9] about the investigation of cycle-to-cycle variations in homogeneous charge compression ignition (HCCI) engines using the well stirred reactor (WSR) model. Adomeit et. al [10] studied the influence of cycle-to-cycle variations of inlet conditions on the fuel-air mixing process in a direct injection spark ignition (DISI) engine. LES simulations employing the progress variable approach (to model turbulent combustion) were used to study turbulent flows in diesel engines [11] and lean ethanol/air mixtures in HCCI engines [12, 13]. Other examples of LES studies of ICE can be found in the review paper of Rutland [14].

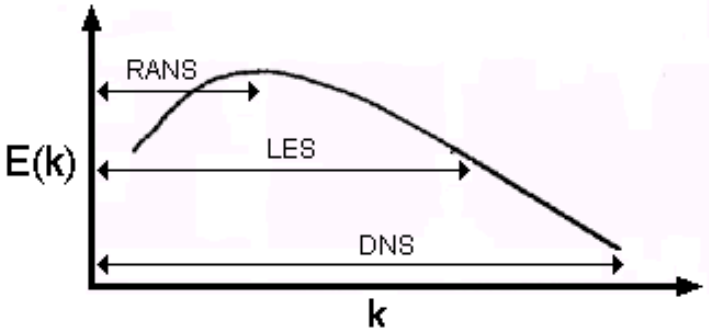

Figure 1: Resolution of the energy spectrum by different approaches [8]. Here, $E(k)$ denotes the turbulent kinetic energy in the wavenumber (k) space.

As ICE emissions regulations are getting stricter, different concepts to improve combustion and reducing tailpipe emissions are being studied. For example, to reduce NOx in spark ignition engines, lean air-fuel mixture is used and to reduce NOx in diesel engines, more exhaust gas recirculation (EGR) is being used. Other concepts of improving combustion by having a low temperature combustion process are also being investigated. Many current turbulent combustion models in CFD assume fast chemistry regimes and are aimed to describe either premixed or non-premixed modes of combustion. However, future engines will most likely operate at lower temperatures, higher pressures, and higher level of air dilution than today's engines. So most combustion models used today might not adequately predict com-

bustion under those operating conditions that take place in unconventional mixed-mode and turbulent combustion regimes. The basic requirement for a mode and regime independent turbulent combustion model is that it should accurately represent the interactions between small and large scale turbulence, chemistry and molecular diffusion.

Combustion models such as WSR and partially stirred reactor (PaSR) model do not take into account the affect of unresolved turbulence on chemistry. There are many ICE studies using these two models, a few examples are [9,15–17]. Chemistry in WSR model depends only on the resolved mean values but still simulations with this model are able to get good agreement with experimental data for diesel, HCCI and dual-fuel combustion engines [18, 19]. In PaSR model, the affect of turbulence on chemistry is taken into account by dividing each CFD cell in two different zones, i.e. one of the zone is considered as well stirred reactor and the other zone has no reactions at all. The size of each zone sub-volume is then determined by the variance of progress variable and mixture fraction. A standard turbulence model provides the turbulent mixing time between the well stirred reactor and the non-reacting zones. The subgrid fluctuations of mixture fraction and progress variable produces a time delay of chemical conversion, which causes the difference of outcomes between PaSR and WSR modeling approaches.

The flamelet approach is another widely used approach, see [2] for details. The flamelet models assume fast chemistry leading to the idea that combustion happens in laminar flame structures carried and stretched by the turbulent flow field. There is a scale separation of chemical and turbulent length and time scales, therefore the affect of turbulence on chemistry is achieved by using parameters, e.g. using scalar dissipation rate in non-premixed combustion. Flamelet models have low computational cost and have been used successfully in both pure premixed [20,21] and non-premixed combustion simulations [22, 23]. Attempts have been made to extend the flamelet models to mode independent combustion models [24–26] but partially premixed combustion mode was not represented properly. As flamelet models rely on fast chemistry assumption, combustion phenomenon under non fast chemistry such as extinction and reignition are not addressed. These particular phenomenon were modeled with extended flamelet models [27, 28] but only under idealized conditions. Therefore, flamelet models cannot be considered as mode and regime independent turbulent combustion models. However, there are vast amount of studies of flamelet models on ICE, see [29–36] for examples.

Another model similar to the flamelet model is the conditional moment closure (CMC) model. This model was introduced by Bilger and

Klimenko [37] and relies on the fact that a reactive scalar conditioned on a conserved scalar does not fluctuate as strongly. Therefore this model relates the fluctuations of all reactive scalars to a conserved scalar, e.g., mixture fraction in non-premixed combustion. The above assumption holds true if the flame is moderately influenced by flow then the conserved scalar does not fluctuate strongly and it is sufficient to use first order closure for the chemical reaction term. In this situation, CMC model is identical to the flamelet model and hence is not mode and regime independent. If the flame is heavily influenced by flow then to overcome inaccurate predictions, second order closure for the chemical reaction term is necessary which would result in high computational costs. That is why ICE studies are only done using first order closure for the chemical source terms. De Paola et al. [38] and Bolla et al. [39] used first order CMC closure in heavy duty diesel engine simulations and the simulation results were in close agreement to the experiments.

Existing mode and regime independent turbulent combustion models include transported PDF (TPDF) [40] and LES-LEM (discussed later). TPDF models use a detailed chemistry description and have been used successfully for many combustion applications. They are more computationally expensive than flamelet models and thus are limited to relatively few reactive scalars chemistry. The mode and regime independent modeling capabilities of TPDF models however, depend on the available micro-mixing models and much work has been done in the past to improve these micro-mixing models. In one-point PDF closure, interaction between turbulence and flame micro-structures depends on modeling and this remains the key limitation of one-point PDF closure. However, TPDF models have been successfully applied to simulate various ICE concepts. Examples include work done by Zhang et al. [41] on HCCI combustion engine and Mohan and Haworth [42] on a heavy duty diesel engine.

One turbulent combustion model which has been successfully applied to both premixed and non-premixed combustion and can be regarded as a truly mode (premixed/non-premixed) and regime (fast/non fast chemistry) independent is the linear-eddy model (LEM) of Kerstein [1] used as a subgrid combustion model for LES called LES-LEM [43, 44].

Kerstein [1] developed LEM with the motivation that, in order to accurately represent turbulent combustion, a model should be able to represent all relevant physical processes, notably turbulent advection, molecular diffusion, and chemical reaction. LEM resolves and simulates on a one-dimensional (1D) line all these processes at their relevant length and time scales hence reducing the computational cost relative to three-dimensional (3D) DNS while retaining high resolution. The effects of realistic 3D tur-

bulence on the LEM scalar fields are modeled via instantaneous mapping events using 3D scaling laws. LEM was initially formulated as a scalar mixing model for non-reacting flows [1] and later extended to predict reactive flows [45]. LEM has been used both as a stand-alone tool and as an LES subgrid combustion model (LES-LEM).

In LES-LEM, physical processes, i.e. large and small scale turbulent advection, molecular diffusion and chemical reaction are modeled at their respective length and time scales. LES solves the large scale mass, momentum and energy equation whereas to capture physics on the unresolved small scale, LEM is used in each LES cell. LEM solves for chemical reactions, molecular diffusion and also models subgrid turbulent advection. LES and LEM are coupled by exchanging some information. Large-scale advection in LES-LEM is modeled by lagrangian mass transfer of LEM between LES cells. LES-LEM has been employed in a large variety of combustion problems [46–58]. McMurtry et al. [59] showed successful simulations of turbulent scalar mixing employing LES-LEM. Non-premixed turbulent combustion simulations were done using LES-LEM by Calhoon [60] and Menon and Calhoon [61], and premixed turbulent combustion by Smith [62] and Chakravarthy and Menon [63]. Spray combustion simulations using LES-LEM were performed by Pannala and Menon [64], and by incorporating radiative heat loss and soot modeling to LES-LEM by Zimberg et al. [65]. Predictions of a premixed turbulent methane/air flame using LES-LEM were presented by Sankaran and Menon [66]. Sen and Menon employed LES-LEM simulations using artificial neural network to successfully speed up chemistry [67,68]. LES-LEM with a low-Mach-number numerical scheme was used to simulate the SANDIA non-premixed piloted methane/air flame D by Ochoa et al. [69]. Choi applied LES-LEM for simulations of a cavity-stabilized combustor [70]. A few examples of simulation on ICE include work done in KIVA for simulating a direct injection spark ignition engine using LES-LEM [71], and an URANS-LEM method in order to investigate pressure histories in a HCCI engine [72]. Martinez et al. [73,74] studied turbulent combustion of hydrogen-enriched fuels by using LES-LEM. Lovett et al. [75] utilized LES-LEM for studying flame structure of bluff-body stabilized flames. Srinivasan et al. [76] used LES-LEM for investigating combustion instabilities in a continuous variable resonance combustor (CVRC) and also performed spray combustion simulations [77]. Because of simulating rather than modeling the interaction of turbulent advection with diffusion and chemical reactions, LES-LEM is capable of predicting extinction and reignition effects which has been demonstrated by Sen et al. in [68].

Turbulent combustion models can be used in at least two different ways [3]. One is the so-called primitive-variable method in which the models pro-

vide closure for the filtered or averaged thermochemical quantities, i.e. the species mass fractions and an energy variable such as enthalpy or temperature. This method is perhaps the most popular one and is typically used with flamelets [2], TPDF methods [78–80], and in most previous LES-LEM studies as well. The other method is the reaction-rate approach in which the turbulent combustion model provides closure for the chemical source terms in the conservation equations of the thermochemical quantities, i.e. these class of models solve transport equations for all species and a form of the energy equation. Thus, this approach is computationally more expensive than the primitive-variable method. However, the approach can be regarded as more broadly applicable as it simplifies the inclusion of more physics into the modeling [3].

An additional advantage of using the reaction-rate approach is that it can potentially ease the use of more than one turbulent combustion model during a simulation. For example, consider a combustion problem involving a vigorously burning flame in some region in spacetime, a flame undergoing extinction-reignition in another region, and ignition in yet another region. This is a multi-physics combustion problem. Knowing the fact that turbulent combustion models can be more cost-effective (e.g. in terms of accuracy and computational cost) for a particular type of physics but not necessarily for other physics, it becomes desirable to use one particularly suitable model for one region in spacetime and other suitable models in other regions. The potential for such an approach to lead to more cost-effective combustion simulations is beginning to be recognized [81, 82]. This is the case not only in the combustion community but, for instance, in the multi-phase-flow community as well [83]. Within this hybrid framework, the primitive-variable method runs into difficulty that turbulent combustion models handle the turbulent transport in different ways. In comparison, the reaction-rate approach does not run into this problem as it solves for the conservation equations of the thermochemical quantities. Furthermore, the reaction-rate approach isolates modeling errors due to the turbulent combustion model in the chemical source terms, simplifying as well the comparison of errors from different models.

The primitive-variable approach is standard for previous LES-LEM implementation so it is valuable then to explore how well a new LEM closure with the reaction-rate approach performs. This thesis introduces a new LEM closure for LES-LEM using the reaction-rate approach. In this closure, a low-Mach-number formulation of LES equations for mass, momentum, sensible enthalpy and species mass are solved in Eulerian form on a 3D LES grid. LEM solves for temperature and species mass on the 1D line inside each LES cell. LEM solves chemical reactions and molecular diffusion

and the subgrid turbulent advection is modeled by LEM by stochastic rearrangement events called triplet maps. The triplet maps represent action of turbulent eddies on the LEM scalars. Another element of the present LES-LEM formulation is modeling of large-scale advection, for which the splicing algorithm is used since it has proven to be robust for practical combustion implementations. The splicing algorithm cuts and pastes the end portions of the 1D arrays of the adjacent LES cells to emulate a Lagrangian type of mass transfer. Decisions of how much to cut and paste are based on values of the mass fluxes across the faces of LES computational cells. For example, if the mass flux at a given face of cell A is large and directed from cell A to cell B, a large portion of the 1D array in A will be cut and then pasted onto one of the two endpoints of the array in B. If this mass flux were small, a small portion would be cut and pasted. A new splicing strategy based on an ordered flux of spliced LEM segments is presented here in this thesis. The principle is that low-flux segments have less momentum than high-flux segments and therefore are displaced less than high-flux segments. This strategy affects the order of both inflowing and outflowing LEM segments of a LES cell. In the present LES-LEM formulation, during each LES time step LES provides information needed to advance the LEM solution and LEM in return provides chemical source terms to LES. These source terms are then used in LES equations for sensible enthalpy and species mass.

In this thesis, LES-LEM predictions with the new closure for a bluff-body stabilized combustor are compared with experiments, WSR model and a traditional LES-LEM study employing the primitive-variable approach. The bluff-body stabilized combustor is a standard test case for the evaluation of turbulent premixed combustion models which has been investigated extensively in the past. The present work makes use of unstructured meshes and a pressure-based approach, both of which are favorable in industry. It is shown that current LES-LEM implementation is robust. Focus is also put on an important part of LES-LEM, i.e. splicing. A dedicated investigation of splicing is done by simulating turbulent passive scalar mixing and by comparing the new splicing strategy with an old one.

This thesis has two chapters. The first chapter describes the model formulation of LES-LEM using the reaction-rate approach. The second chapter focuses on the combustion simulations using LES-LEM and the dedicated investigation of splicing by doing the mixing simulations.

Chapter 1

Model formulation

1.1 Introduction

This chapter describes the LES-LEM model in detail. The LES-LEM model is composed of the following elements: the LES equations (section 1.2), the LEM modeling inside a LES cell (section 1.3), the large-scale advection modeling by splicing (section 1.4) and for the current formulation the closure of the chemical source terms and exchange of information between the LEM and the LES (section 1.5).

The governing conservation equations for mass and momentum are:

$$\frac{\partial \rho}{\partial t} + \frac{\partial (\rho u_i)}{\partial x_i} = 0 \,, \tag{1.1}$$

$$\frac{\partial \rho u_i}{\partial t} + \frac{\partial (\rho u_j u_i)}{\partial x_j} = -\frac{\partial p}{\partial x_i} + \frac{\partial}{\partial x_j} \left(\tau_{ji} \right) \,. \tag{1.2}$$

Here ρ denotes the density, p the pressure, u_i is the velocity component in spatial direction i and τ_{ji} the viscous stress tensor.

In LES, the three common filters include a cut-off filter in spectral space, a box (top-hat) filter in physical space and a Gaussian filter in physical space [3]. The current work uses the implicit top-hat filter.

1.2 LES equations

The current work uses the OpenFOAM library version 2.3.1 [84,85] and considers the following filtered conservation equations for global mass, momentum, sensible enthalpy, and species mass for gases that are variable density, viscous, heat-conducting and multiple-component and move at low-Mach-number speeds:

$$\frac{\partial \bar{\rho}}{\partial t} + \frac{\partial (\bar{\rho} \tilde{u}_i)}{\partial x_i} = 0 \,, \tag{1.3}$$

$$\frac{\partial \bar{\rho} \tilde{u}_i}{\partial t} + \frac{\partial (\bar{\rho} \tilde{u}_j \tilde{u}_i)}{\partial x_j} = -\frac{\partial \bar{p}}{\partial x_i} + \frac{\partial}{\partial x_j} \left(\bar{\tau}_{ji} + \tau_{ji}^{sgs} \right) \,, \tag{1.4}$$

$$\frac{\partial \bar{\rho} \tilde{h}}{\partial t} + \frac{\partial (\bar{\rho} \tilde{u}_j \tilde{h})}{\partial x_j} = -\frac{\partial}{\partial x_j} \left(\bar{q}_j + q_j^{sgs} \right) + \bar{S}_h \,, \tag{1.5}$$

$$\frac{\partial \bar{\rho} \tilde{Y}_\alpha}{\partial t} + \frac{\partial (\bar{\rho} \tilde{u}_j \tilde{Y}_\alpha)}{\partial x_j} = -\frac{\partial}{\partial x_j} \left(\bar{j}_{\alpha,j} + j_{\alpha,j}^{sgs} \right) + \bar{S}_\alpha \,. \tag{1.6}$$

Here h is the sensible enthalpy, and Y_α is the mass fraction of the species α. The bar denotes conventional filtering and the tilde denotes density weighted Favre filtering. $\bar{\tau}_{ji}$, $\bar{q}_j$, and $\bar{j}_{\alpha,j}$ are respectively the filtered viscous stress tensor, heat flux, and Fickian molecular flux of species α. Likewise,

τ_{ji}^{sgs}, q_j^{sgs}, and $j_{\alpha,j}^{sgs}$ are the subgrid viscous stress tensor, heat flux, and molecular flux of species α, all of which need closure. These conservation equations are complemented with the equation of state for ideal gases

$$\overline{p} = \overline{\rho} R_m \sum_{\alpha=1}^{N} \frac{\tilde{Y}_\alpha \tilde{T}}{W_\alpha} \ , \tag{1.7}$$

where W_α is the molecular weight of species α and R_m is the universal gas constant. The averaged caloric equation of state is given as,

$$\tilde{h} = \tilde{h}(\tilde{T}) \ = \sum_{\alpha} \tilde{Y}_\alpha h_\alpha(\tilde{T}) \tag{1.8}$$

with $h_\alpha(T)$ given by the NASA polynomials.

The terms τ_{ij}^{sgs}, q_j^{sgs}, and $j_{\alpha,j}^{sgs}$ are the subgrid stress tensor, heat flux, and mass flux of species α. They are closed with

$$\tau_{ij}^{sgs} = -2\mu^{sgs} \left(\widetilde{S}_{ij} - \frac{\delta_{ij}}{3} \widetilde{S}_{kk} \delta_{ij} \right) \ , \tag{1.9}$$

$$q_j^{sgs} = -\frac{\mu^{sgs}}{\overline{\rho}} \frac{\partial \widetilde{h}_s}{\partial x_j} \ , \tag{1.10}$$

$$j_{\alpha,j}^{sgs} = -\frac{\mu^{sgs}}{\overline{\rho}} \frac{\partial \widetilde{Y}_\alpha}{\partial x_j} \ . \tag{1.11}$$

μ^{sgs} is computed with OpenFOAM's implementation of Yoshizawa & Horiuti's one-equation eddy model [86].

1.3 LEM subgrid modeling inside a LES cell

The hallmark feature of the LEM is a 1D domain resolving all scales [44]. In LES-LEM there is one LEM line per computational LES cell, as shown in Fig. 1.1. Each LEM line inside LES cells has an inflow on one end and an outflow at the other end. Each LEM line in a LES cell is divided into LEM cells and all these LEM cells are uniformly initialized with the thermochemical conditions in that LES cell. The initial LEM length is chosen to be equal to the local LES mesh spacing Δ. The solution on the LEM is governed by, among others, the conservation equations in their 1D form as:

$$\sum_i \rho_i \Delta x_i = M_{LEM} \ , \tag{1.12}$$

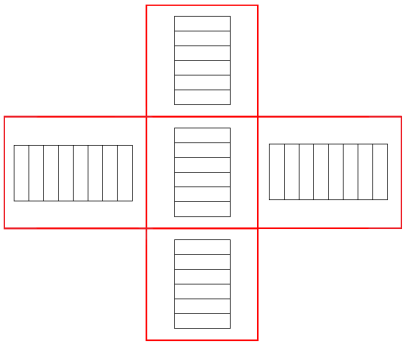

Figure 1.1: LES-LEM simulations use a 1D domain (in black) consisting of a stack of LEM cells per computational LES cell (in red) [87]. Note that the LEM domains have no assigned orientation relative to the underlying coordinate system.

$$\frac{\partial T}{\partial t} = -\frac{\partial q_x}{\partial x} + S_T \ , \tag{1.13}$$

$$\frac{\partial Y_\alpha}{\partial t} = -\frac{\partial j_{\alpha,x}}{\partial x} + S_\alpha \ , \tag{1.14}$$

where M_{LEM} is the total mass in a LEM line, the summation (index i) is done over all cells of the LEM domain, the x coordinate is parallel to the 1D line, and S_T is the heat-source term in the temperature equation. Constant pressure is assumed on the LEM which allows updating of the LEM density. Unity Lewis number is used to compute q_x and $j_{\alpha,x}$.

Subgrid-scale turbulent advection (stirring) is modeled by the triplet maps, which mimic the action of turbulent eddies on the subgrid scalar field. Figure 1.2 taken originally from [47] shows the modelling of eddies using triplet maps. The top of Figure 1.2 shows a plane material surface having separate species A and B. The horizontal lines represent the initial concentration isopleths. Also initially, the concentration profile is uniform gradient shown by the straight line in the dashed box. The bottom part of Figure 1.2 shows the action of an eddy on the concentration isopleths.

The scalar field after triplet mapping is continuous and the map is measure preserving, which means that triplet maps do not create or destroy mass or energy but just re-arrange the scalar data on the 1D LEM line. The mapping procedure first makes three copies of the selected LEM segment (which represents the region affected by an eddy) and then each copy is compressed by a factor of 3. Lastly the middle copy is flipped to ensure a continuous profile. This is how the rotational and compressive motions observed in the turbulent flows are represented in the LEM [88].

The triplet mapping needs three parameters to specify an eddy event,

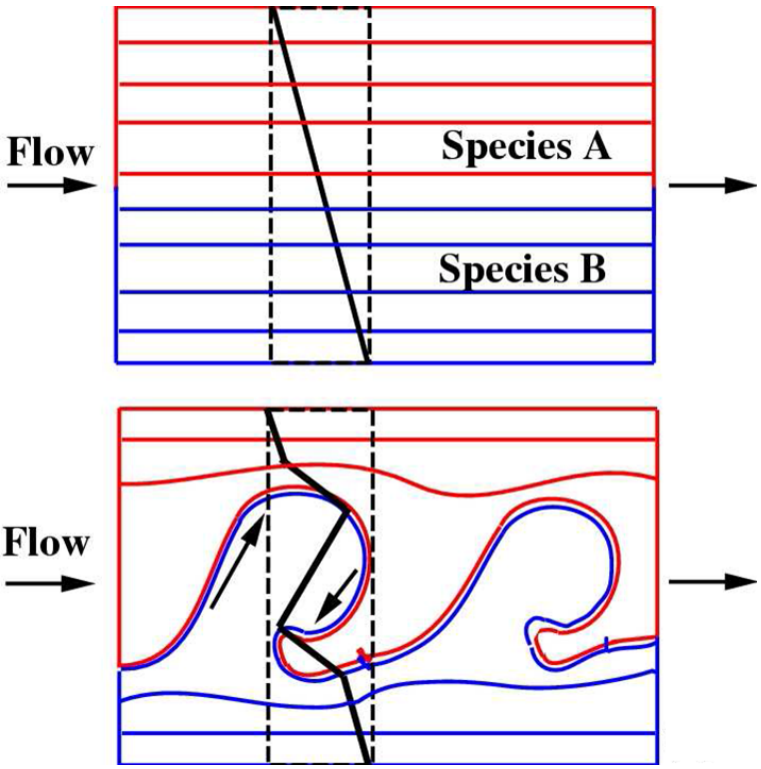

Figure 1.2: Schematics of the effect of an eddy [47]

i.e. an eddy location x_0 within the LEM domain, eddy length l, and an eddy rate λ per unit domain length. The eddy location x_0 is sampled in a stochastic way from a uniform distribution.

If $f(l)$ denotes the probability density function of the eddy sizes, then the turbulent diffusivity D_T is given by [89]:

$$D_T = \int_{l_p}^{l_{max}} \frac{2}{27} \lambda l^3 f(l) dl \ , \tag{1.15}$$

where l_p and l_{max} are the smallest and the largest unresolved length scales characterizing the turbulence, and are specified by the user. Here l_p is taken as the Kolmogorov length scale η and $l_{max} = \Delta$. The turbulent diffusivity D_T scales with $l^{4/3}$ [89–91] resulting in:

$$f(l) = \frac{5}{3} \frac{l^{-8/3}}{\eta^{-5/3} - \Delta^{-5/3}} \ , \tag{1.16}$$

An estimate for the Kolmogorov length scale is given by

$$\eta = N_\eta \frac{\Delta}{Re_\Delta^{3/4}} \ , \tag{1.17}$$

with N_η being a model constant, and Re_Δ the subgrid Reynolds number:

$$Re_\Delta = \frac{u_{sgs}\Delta}{\nu} \,, \tag{1.18}$$

where ν is the kinematic viscosity and u_{sgs} is the characteristic subgrid velocity fluctuation obtained from the LES subgrid turbulent kinetic energy $\bar{k}_{sgs}$ as $u_{sgs} = \sqrt{2\bar{k}_{sgs}/3}$.

The eddy rate λ with unit (length x time)$^{-1}$ is obtained by inserting Eq. 1.16 in to Eq. 1.15 as shown in [89]

$$\lambda = \frac{54}{5}\frac{\nu Re_\Delta}{C_\lambda \Delta^3}\frac{\left(\frac{\Delta}{\eta}\right)^{5/3} - 1}{1 - \left(\frac{\eta}{\Delta}\right)^{4/3}} \,, \tag{1.19}$$

with C_λ being a model constant. The average time interval between triplet maps is:

$$\Delta t_{stir} = \frac{1}{\lambda l_{LEM}} \,. \tag{1.20}$$

where l_{LEM} is the LEM domain length and the actual eddy occurrences are sampled from a Poisson process. The sampling rejected the eddies that extend beyond the LEM domain boundary. The values of $C_\lambda = 1$ and $N_\eta = 1.1$ are used. These values were chosen to ensure that triplet maps are being observed during the simulation.

1.4 Large-scale advection modeling

On the LES, large-scale advection is simply the resolved flow which transports/advects small-scale structures across LES cell boundaries. As small-scale structures are represented on the LEM, a splicing procedure represents large-scale advection for the LEMs. Splicing satisfies conservation of mass and transports mass across LES cell faces in a Lagrangian way. Splicing accounts for mass fluxes across LES cell faces and is implemented via Lagrangian transport of LEM cells between LES control volumes. This method requires three quantities:

1. The magnitude of mass to be transported across each LES cell face,

2. The direction of mass transport on each LES cell face i.e. outflux or influx,

3. An algorithm for ordering of the splicing operations.

Total mass to be transferred across each LES cell face has two contributions, a subgrid mass due to the unresolved velocity fluctuation and a resolved mass due to the resolved velocity. The subgrid mass contribution is given by:

$$M_{sgs} = \frac{\Delta t A_{LES} u_{sgs}}{V_{LES}} M_{LEM}, \tag{1.21}$$

where A_{LES} is the LES face area. V_{LES} and M_{LEM} denote the LES cell volume of splicing donor and the total mass of LEM line of splicing donor, respectively. The direction of the subgrid mass contribution is chosen randomly.

The resolved mass contribution for total splicing mass is given in analogy to Eq. 1.21 by:

$$M_{res} = \frac{\Delta t A_{LES} u_{LES}}{V_{LES}} M_{LEM}, \tag{1.22}$$

where u_{LES} is the LES resolved velocity on the LES cell face. The direction of the resolved mass contribution is given by the direction of u_{LES}.

Fig. 1.3 illustrates the splicing process.

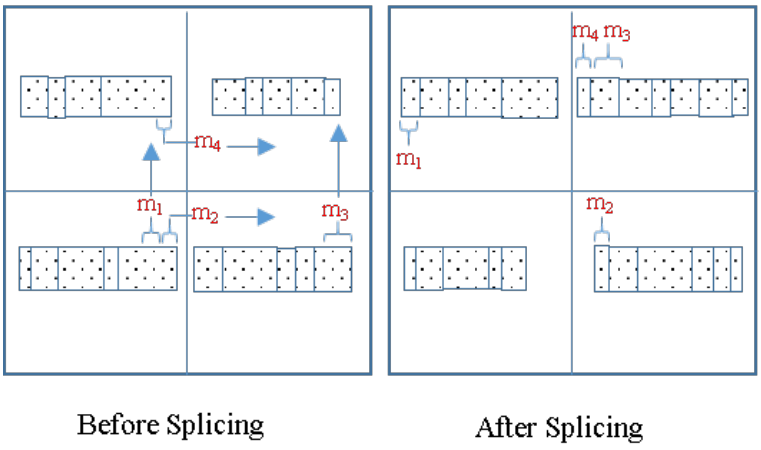

Figure 1.3: Schematics of the splicing process.

The sum of Eqs. 1.21 and 1.22 gives the mass to be transferred across an LES cell face during splicing. Also the direction of transfer is determined, so the face has an outflow and an inflow side. The LEM domain in the outflow cell provides the needed mass. This is done by removing a contiguous interval (segment) of the LEM domain on the outflow side of the LES cell face and attaching it to the LEM domain on the inflow side of the LES cell face.

Because each LES cell has many faces, there will typically be multiple outflows and inflows associated with a given LES cell. Some rationale

is needed to determine the locations and sequencing of the removals and attachments of the segments crossing the various faces of a given LES cell.

This depends first on the chosen structure of the LEM domain. Topologically, the choices are a loop, corresponding to periodic boundary conditions, or a line segment. Here, as in most of the cited previous work, a line segment is used, with input and output sites at the respective endpoints of the line segment. This is a desirable choice because it tends to enforce consistency of the residence time of LEM fluid elements, which extends from the time of attachment to the LEM domain to the time of eventual removal. This point is illustrated by considering the alternative choice of attaching and removing fluxed segments at the same endpoint. Then the residence-time distribution would be highly skewed, with a strong peak at short residence time and a long tail reflecting fluid retained for a long time near the other endpoint, which is effectively an unphysical stagnation point. This is not only counter-intuitive, but introduces model artifacts. In Eulerian schemes, the Courant-Friedrichs-Lewy (CFL) constraint is associated with the requirement that fluid should not be algorithmically propagated through multiple control volumes during one time step. This is a numerical instability mechanism as well as unphysical. Attachment and removal at the same LEM endpoint could propagate some fluid through multiple control volumes during one time step because the total number of attachments and removals per LEM domain equals the number of LES cell faces, which is six in a Cartesian mesh and typically more in an unstructured mesh, allowing a possible 'bucket brigade' scenario. Avoidance of this would require time step reduction far below the permissible CFL time step for an Eulerian transport scheme.

The mean residence time is dictated by the LES-prescribed mass-flux time history, so the degree of freedom available to avoid this artifact is the residence-time distribution, which should be as narrow as possible to minimize residence-time fluctuations. Designating each LEM domain endpoint as solely an input or an output location assures that fluid must pass through the domain between its attachment and removal times, thus avoiding the short-residence-time scenario.

1.4.1 New splicing algorithm

The new splicing approach links the subgrid LEM implementation to the concept of control-volume crossing rate. The direction of the crossing rate is implied by the direction of the LES-prescribed mass fluxes. High flux implies high crossing rate, corresponding to high displacement per time step, and vice versa. High flux also implies the transfer of a relatively large

mass of the LEM domain across an LES cell face. It follows that larger mass transfers undergo more displacement, and vice versa, as illustrated in Fig. 1.4.

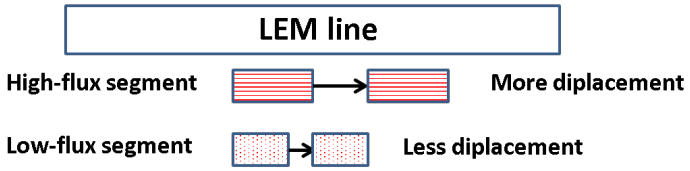

Figure 1.4: Principle of the new splicing algorithm

Figs. 1.5 and 1.6 show how this principle is applied to the sequencing of segment removals and attachments during splicing. The segments to be spliced are considered as flowing along the LEM domain (meaning starting from the domain state prior to modification by splicing) and being ejected from the domain through the output boundary, and thus available for transfer across an LES face. For the lower-flux segments to flow a shorter distance than the higher-flux segments, they need to be closer to the output boundary and the high-flux segments need to be farther from that boundary. This implies that the ordering of removal is first the lowest-flux segments and then the higher-flux segments as shown in Fig. 1.5.

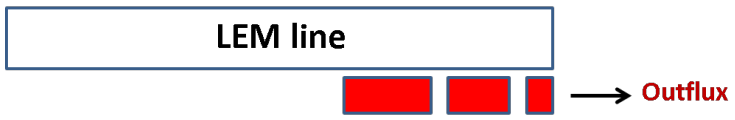

Figure 1.5: Order of removal of the LEM segments from the output boundary on the basis of flux

Using the same principle, the highest-flux segments are attached first to the inflow side of LEM line, followed by the lower-flux segments as shown in Fig. 1.6.

Figure 1.6: Order of joining of the LEM segments to the input boundary on the basis of flux

Further implementation details are as follows and summarized in Fig. 1.7. The new splicing algorithm is implemented by looping three times over all

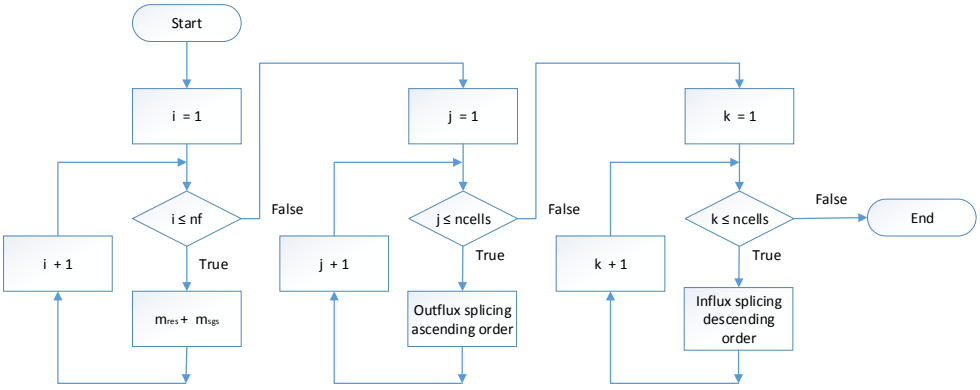

Figure 1.7: The new splicing algorithm implementation. Here nf and ncells denote the total (in whole computational domain) number of LES cell faces and LES cells respectively.

LES cells in the whole computational domain. During the first loop, the magnitude and direction of mass flux on each LES cell face are calculated. An empty list is attached to each LES face. In the second loop, all outflux faces of an LES cell are identified and their respective outflux masses are gathered and sorted in ascending order. Then the outflux LEM segments corresponding to the outflux masses are spliced (cut and paste) in ascending order of outflux mass from the splicing donor LEM line to the corresponding empty lists (attached to each LES face). This procedure is repeated for all other LES cells until the second loop is finished and all the empty lists are now filled. Using the same principle, in the third loop, all the influx faces of a LES cell are recognized and their respective influx masses are sorted in descending order. Then the LEM segments are spliced in descending order (of influx mass) to the splicing receiver LEM line from the corresponding filled lists (attached to each LES face). The third loop goes through all LES cells and in the end all the filled lists resulting from the second loop are empty again. The splicing process is complete.

1.4.2 Parallel splicing

LES-LEM is computationally expensive and is not feasible without parallel computation. The standard splicing algorithm on a single processor domain has been implemented very efficiently using a pointer based LEM data structure where splicing is realized via simple pointer re-arrangements. However, domain decomposition for parallel computations on distributed memory architectures leads to processor domains which have a priori no input from

neighboring processor domains. If splicing is not done correctly (e.g. by a simplified cell averaged approach) at processor boundaries, it can lead to unphysical results.

In order to perform splicing across processor boundaries, LEM lines across processor boundaries (called ghost LEM lines) are copied to the neighboring processor. Then splicing is performed between LEM lines that are next to the boundary and the ghost LEM lines by each processor.

1.4.3 Splicing at inlet and outlet boundaries

For LES cells at the inlet boundary, inlet mass needs to be added to their respective LEM lines. This inlet spliced mass is calculated using the same Eqs. 1.21 and 1.22 and is added on the influx side of the LEM line. The remaining properties of this added fluid are taken from the inlet boundary. For inlet splicing mass calculations, the direction of the subgrid mass contribution (Eq. 1.21) is taken to be influx.

For the outlet boundaries, the calculated outlet splicing mass is removed from the outflux side of the LEM line. For outlet splicing mass calculations, the direction of the subgrid mass contribution (Eq. 1.21) is taken to be outflux.

1.5 Closure of the chemical source terms with LEM

Fig. 1.8 shows the coupling between the LES and the LEM subgrid combustion model. The LES provides information about the cell spacing Δ, the subgrid turbulent kinetic energy $\bar{k}_{sgs}$, the time step of the simulation Δt and the pressure to the LEM. With this information, the LEM subgrid-scale simulation advances Eqs. 1.12-1.19 for the LES time interval Δt. The chemical source terms $\bar{S}_h$ and $\bar{S}_\alpha$ are obtained by taking the median value along various LEM elements for the current LES time step. The median source term is calculated by first sorting the source term values of all the LEM cells in ascending order, and then picking up the middle value. The median is a robust measure since it prevents outliers. These source terms are then used in the LES conservation equations for the species mass fractions and sensible enthalpy. The temperature on the LES side is then calculated from the caloric equation of state, Eq. 1.8.

In the present implementation, the PISO algorithm for pressure-velocity coupling [92] is used. It has an outer loop which starts with predicting a velocity (using Eq. 1.4), which is followed by an inner iterative loop to correct the velocity field using the outcome of a pressure Poisson equation

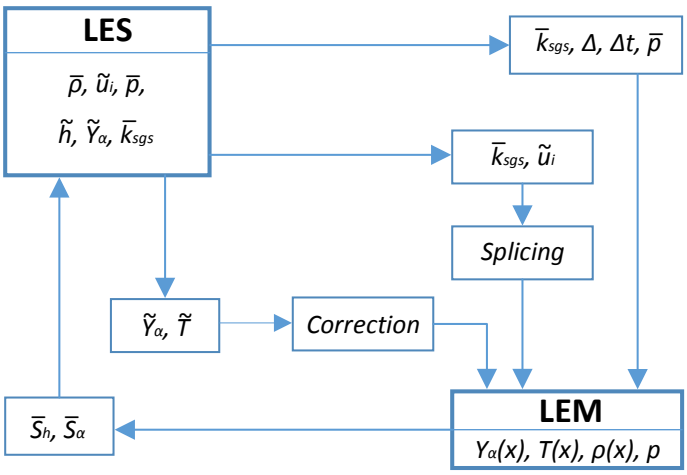

Figure 1.8: Coupling between the LES and the LEM subgrid model.

obtained by fulfilling the continuity equation. In the inner iterative loop, the LES density is obtained from the equation of state Eq. 1.7. Splicing is done with the correct LES velocity resulting from the PISO loop.

The last step shown in Fig. 1.8 is to correct the temperatures and the species mass fractions in the LEM domains to take into account the fact that the convection due to the solution of Eqs. 1.3-1.6 differs from that of the splicing algorithm. This difference is not surprising because the convection of species by the solution of Eq. 1.6 differs from that produced by the splicing in at least two ways. First, the solution of Eq. 1.6 numerically smears the species in a way that the splicing is not prone to because the splicing corresponds to diffusion-free advection in a Lagrangian way. Second, the splicing produces an artifact [93] that the solution of Eq. 1.6 is not prone to.

There is not a unique way to conduct this correction of the temperatures and the species mass fractions in the LEM domains, and the following algorithm is a result of trial and error and has been found to be robust. The goal of this correction algorithm is to keep the Favre-averaged temperatures and species mass fractions from the LEM domains within some tolerance of those from the solution of Eqs. 1.3-1.6. LES quantities are not altered. Fig. 1.9 summarizes the correction for the temperature. A similar process is used for the species mass fractions.

The first step of the correction computes the difference T' between the LES temperature $\tilde{T}$ and the Favre-averaged LEM temperature $\tilde{T}_{LEM}$, the

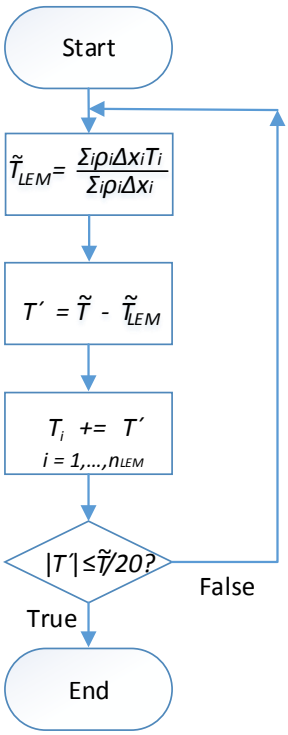

Figure 1.9: Steps of correcting the temperature in a LEM domain. Here T_i is the temperature of LEM cell i and n_{LEM} is the total number of LEM cells. The temperature difference T' is a difference between the LES temperature $\tilde{T}$ and the Favre-averaged LEM temperature $\tilde{T}_{LEM}$.

latter of which is obtained via:

$$\tilde{T}_{LEM} = \frac{\sum_i \rho_i \Delta x_i T_i}{\sum_i \rho_i \Delta x_i} \,, \tag{1.23}$$

where T_i denotes the LEM cell temperature, and summation (index i) is over all cells of the LEM line. In the second step, T' is added to each T_i and this results in updated $\tilde{T}_{LEM}$. If the new updated difference T' is within a specified tolerance, the correction is stopped, otherwise the updated difference T' is added again to each T_i and the aforementioned steps are repeated.

It is important to highlight a distinctive conceptual feature of the present LEM closure using the chemical source terms. It is common in LES to make a sharp distinction between the closure of diffusive processes (micro-mixing) and reaction. This is evident by noticing that in Eqs. 1.3-1.6 separate closure

is needed for, on one hand, $\bar{q}_j$ and $\bar{j}_{\alpha,j}$, and, on the other hand, $\bar{S}_h$ and $\bar{S}_\alpha$. However, a more realistic picture is that diffusive and reacting processes are closely coupled at the subgrid level (meaning reaction and diffusive terms can be of the same order), for example, in some premixed flames. Now, with LEM $\bar{S}_h$ and $\bar{S}_\alpha$ are computed as explained above using a 1D structure that represents both reaction and diffusion. Thus, it is perhaps more accurate to say that the present closure, although given for $\bar{S}_h$ and $\bar{S}_\alpha$, is not a closure for subgrid reaction, but for subgrid reaction-diffusion processes, i.e. with proper resolution the LEM is capable of fully resolving flame structures in 1D. This is why the present LEM closure can also be called as subgrid reaction-diffusion closure with LEM.

Chapter 2

Model validation

2.1 Introduction

This chapter presents in section 2.2, the combustion simulations performed with the present LES-LEM formulation. The dedicated splicing investigation is discussed in section 2.3.

2.2 Combustion simulations

The experimental setup of the bluff-body stabilized combustor [94–96] called Volvo combustor from now on consists of a rectilinear channel, with an inlet section where air and (gaseous) propane mix before entering a honeycomb, and a downstream section where the premixed reactants burn in a flame that gets stabilized downstream of a wedge [94]. The cross section of the wedge is an equilateral triangle with side of 40 mm. The end of the downstream section is connected to a round exhaust duct with a cross sectional area about 3.4 times larger than that of the channel [97]. Atmospheric conditions are used.

The computational domain used for the current work is shown in Fig. 2.1 and has the following geometric parameters: $h_1 = 40\,\text{mm}$, $h_2 = h_1 sin60$, x_{min} = -820 mm, $x_{max} = 680\,\text{mm}$, y_{min} = -60 mm, $y_{max} = 60\,\text{mm}$, and a spanwise length of 40 mm. The honeycomb is ignored as done in previous CFD studies. The pressure gradient normal to the inlet plane is set to zero. No turbulent fluctuations are imposed at the inlet because the region of interest is downstream of the wedge which is responsible for generation of strong turbulence. All walls are modeled as no-slip and non-adiabatic. At the outlet, velocity, temperature and species are set to a zero-normal-gradient condition or a fixed value, depending on the direction of the flow. Pressure is dealt with a similar way at the outlet. Cyclic boundary conditions are used in the z-direction. A non-uniform 3D mesh with 77400 cells is used as well as a tetrahedral 3D mesh with 101134 cells. With the former a time step of 1x10^{-6} s is used, while a time step of 4x10^{-7} s is used with the latter mesh.

The conservation Eqs. 1.3-1.6 are solved with an adaptation of reactingFoam which is the standard solver of the OpenFOAM library for chemically reacting flow. This solver is transient, pressure-based and can handle unstructured meshes [98]. A low-Mach-number assumption is used as done in reactingLMFoam [99, 100] by splitting the pressure into a fluid-mechanical-induced pressure and a thermodynamic pressure, the latter of which is spatially constant and which is used to evaluate the equation of state. As a result, acoustic waves are eliminated from the solution. The time discretization is done with a second-order backward-differencing scheme that

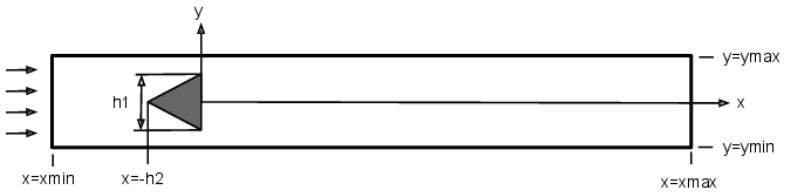

Figure 2.1: Schematic of the Volvo test problem.

Table 2.1: Summary of the simulation settings for case 1

Simulation No.	Denomination	Mesh	C_λ	Correction
1	WSR model	Hexahedral	NA	NA
2	LES-LEM baseline	Hexahedral	1	on
3	LES-LEM $C_\lambda = 10$	Hexahedral	10	on
4	LES-LEM correction off	Hexahedral	1	off
5	LES-LEM tetra	Tetrahedral	1	on
6	PaSR tetra	Tetrahedral	NA	NA

uses the current and previous two time step values. OpenFOAM's limited linear differencing scheme is used for the convective and diffusive fluxes. μ^{sgs} is computed with OpenFOAM's implementation of Yoshizawa & Horiuti's one-equation eddy model [86].

Of the various operating conditions of the Volvo test problems, the one considered for the present work is the so-called case 1. In case 1, the inlet conditions are 288 K temperature, 17 m/s velocity, and 0.61 equivalence ratio. Tab. 2.1 summarizes the various simulations conducted for the present study. A single-step chemical reaction mechanism is used.

2.2.1 Comparison with experiments and WSR model

Fig. 2.2 shows instantaneous temperature maps for the case 1 using the WSR model (simulation 1 cf. Tab. 2.1) and the LES-LEM baseline case (simulation 2 cf. Tab. 2.1). Notice that right downstream of the flame-holder the flame is symmetric about the $y = 0$ plane. This agrees with experiments [96] and many other simulation studies. However, the transition towards an asymmetric flame shape further downstream agrees with some simulation studies [101–103] and disagrees with others where the flame is predominantly symmetric all the way towards the outlet [104–106]. This latter predominantly symmetric shape seems to be the physically correct one

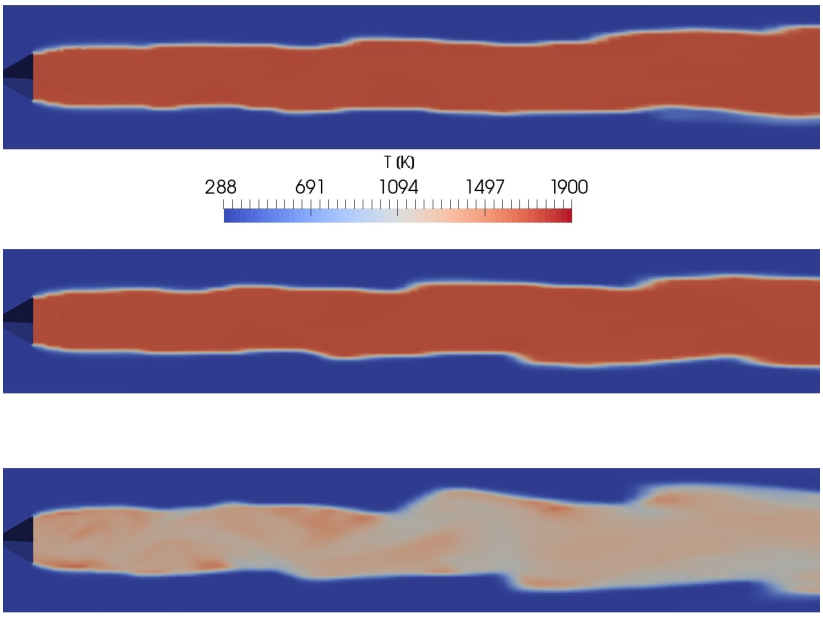

Figure 2.2: Case 1 instantaneous temperature maps with the WSR model (top), the LES-LEM baseline case (center), and a LES-LEM case without the correction (bottom), cf. Tab. 2.1.

for the present boundary conditions because many of the most recent simulation studies show this shape [107–111]. The use of a low-Mach-number formulation instead of a fully-compressible one [109] in the present study may be the cause for the transition from symmetric to asymmetric flame shape seen in the present simulations. Furthermore, it must be stressed that, from the open literature, it is unclear how the flame looks like close to the outlet in the experiments. Fig. 2.2 also compares the effect of the correction step, cf. Figs. 1.8 and 1.9. Notice in Fig. 2.2 that by not using this correction there is an artificial extinction of the flame. Thus, the correction step or some alternative is required.

Spatial variations of mean quantities are shown in Figs. 2.3 and 2.4 for the WSR model (simulation 1 cf. Tab. 2.1) and LES-LEM with C_λ =1 (simulation 2 cf. Tab. 2.1) and 10 (simulation 3 cf. Tab. 2.1). These quantities are averaged in the spanwise direction and over time, the latter of which is done for a time interval of 0.02 s. Overall, Figs. 2.3 and 2.4 show that the sensitivity to the type of model and LES-LEM model constant is small, although the best agreement with the experiments is given by the LES-LEM simulation with C_λ =10. In Fig. 2.3, the largest disagreement

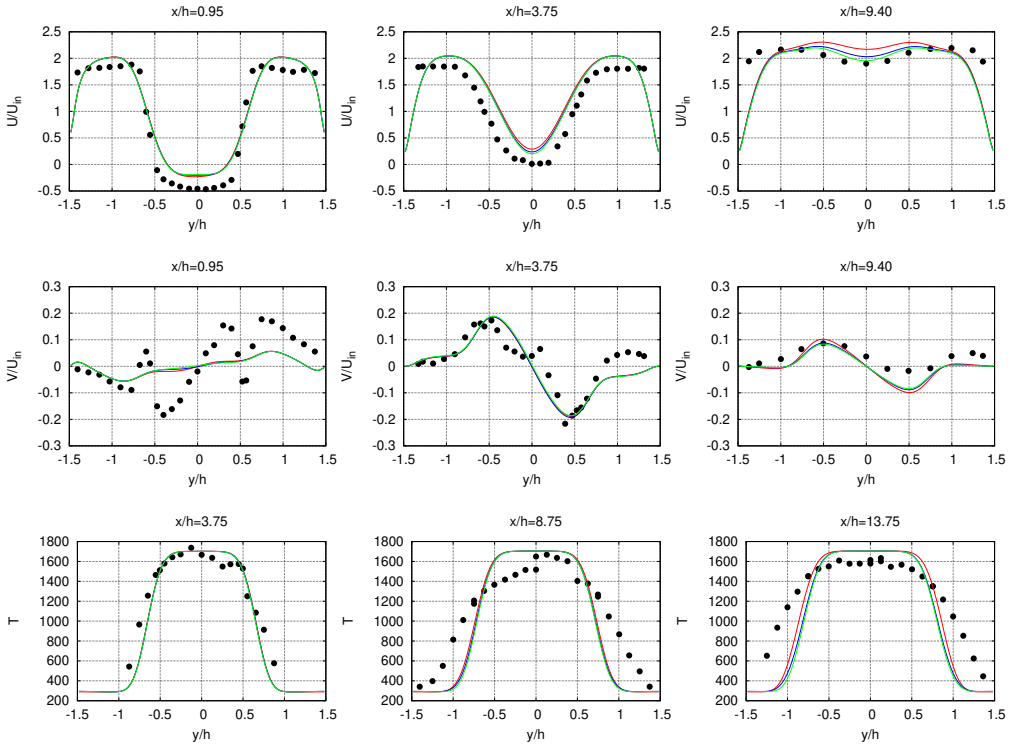

Figure 2.3: Vertical profiles of mean quantities for the case 1 at different streamwise locations obtained with the WSR model (red) and the LES-LEM with $C_\lambda = 1$ (blue) and $C_\lambda = 10$ (green), cf. Tab. 2.1. The experimental data is denoted with black circles. Here, U denotes the mean horizontal velocity, V the mean vertical velocity and U_{in} is the inlet velocity of 17 m/s.

between the experimental data and predictions is seen in the temperature profiles near the outlet. This disagreement could be due to the lack of near-wall mesh refinement in the present simulations, or due to the fact that the wall thermal boundary condition from the experiments is unknown. Nonetheless, the overall agreement between the simulations and experiments shown in Figs. 2.3 and 2.4 is within that seen in some simulation studies [102, 104–106, 112] but slightly less accurate as those seen in other studies [48, 113], the latter of which includes a previous LES-LEM study which is compared to the current study in next Sec. 2.2.2.

Fig. 2.5 shows the vertical variation of rms quantities computed from the resolved fields using the WSR model and the LES-LEM simulations. Close to the flameholder, the largest discrepancy between simulations and experimental results is seen. This discrepancy is not surprising due to the rather coarse mesh used. In addition, Fig. 2.5 shows that the sensitivity of

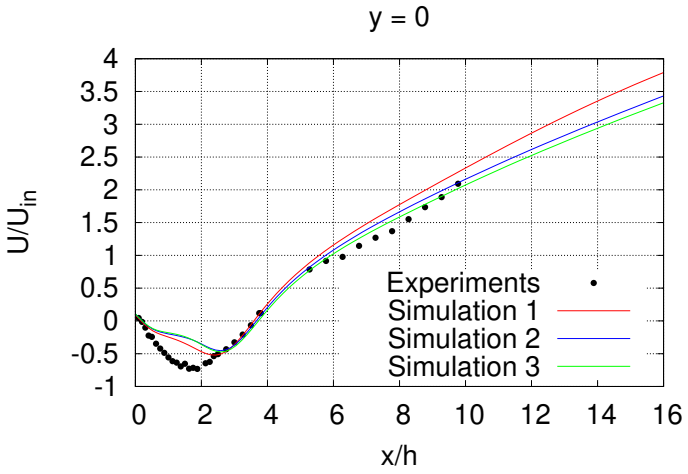

Figure 2.4: Streamwise profiles of the mean horizontal velocity at the $y = 0$ plane for the simulations in Fig. 2.3. For the simulation numbers, cf. Tab. 2.1.

rms quantities to the choice of the turbulent combustion model and LES-LEM model constant is small, except for the rms values of the horizontal velocity at $x/h = 9.4$, where the LES-LEM model with C_λ =10 gives the best agreement with experiments. The LES-LEM model not showing a more accurate prediction than the WSR model in the current tested low Reynolds number Volvo test problem could be due to the subgrid LEM being not so active. It has been shown in another test case [93] that by increasing the Reynolds number, the subgrid LEM became very active.

2.2.2 Comparison with traditional LES-LEM

Fig. 2.6 shows the comparison of the results obtained from the present LES-LEM implementation with the LES-LEM study of Porumbel and Menon [48] which employed the primitive-variable approach. It can be seen that predictions from Porumbel and Menon seem to be slightly more accurate. However, their study employs more than ten times the LES cells used in the present study. Thus, the present study puts LES-LEM model through a more stringent test since a larger portion of the inertial range physics needs to be captured by the 1D LEM and is not directly resolved by the LES.

The present LES-LEM code can handle unstructured meshes which can be seen in Fig. 2.7. This is the first and only implementation of LES-LEM on arbitrary unstructured meshes. When using a very coarse tetrahedral mesh, Fig. 2.7 shows that a prediction with the present LES-LEM model

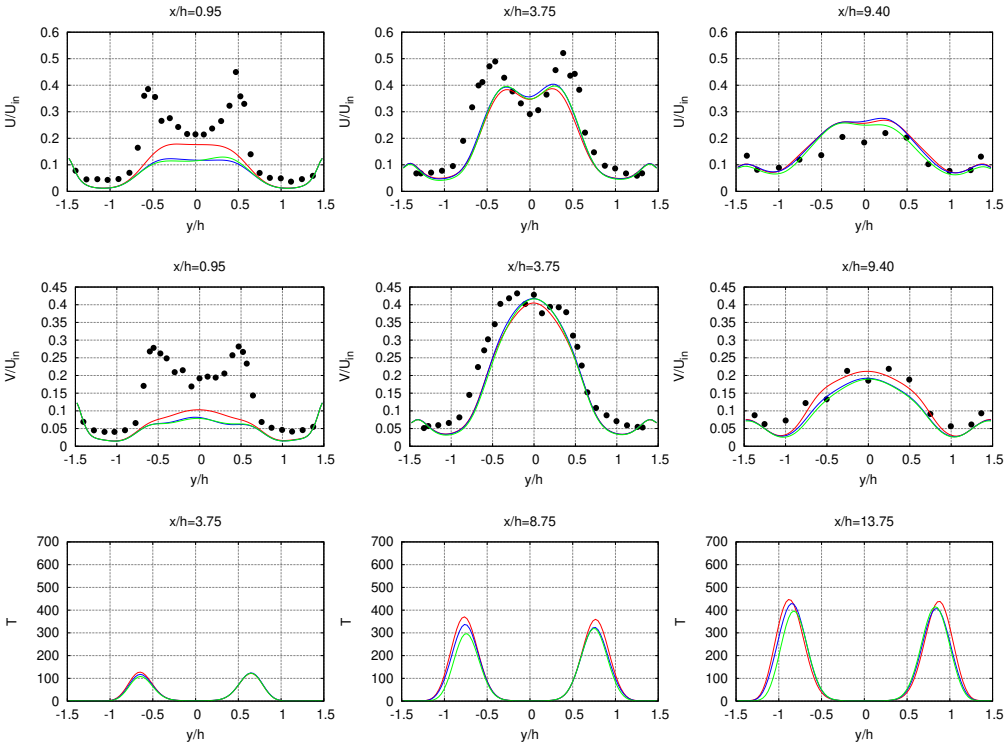

Figure 2.5: Vertical profiles of rms quantities for the case 1 at different streamwise locations obtained with the WSR model (red) and the LES-LEM with $C_\lambda = 1$ (blue) and $C_\lambda = 10$ (green), cf. Tab. 2.1. The experimental data is denoted with black circles.

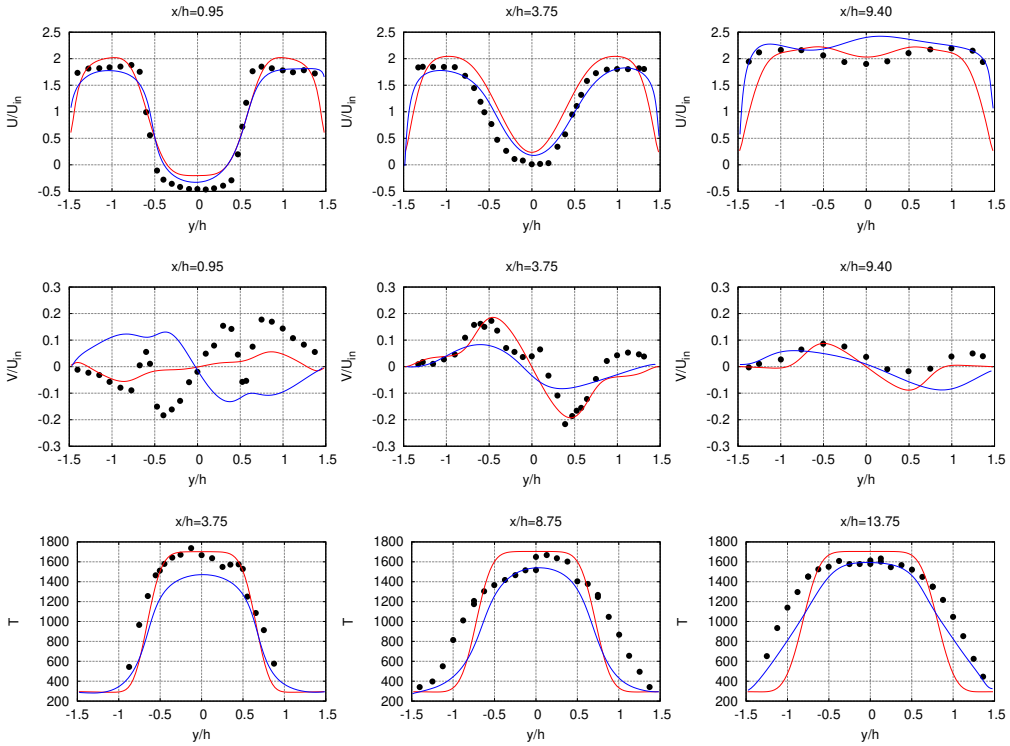

Figure 2.6: Vertical profiles of mean quantities for the case 1 at different streamwise locations obtained with the present LES-LEM study (red) and the LES-LEM of Porumbel and Menon (blue). The experimental data is denoted with black circles.

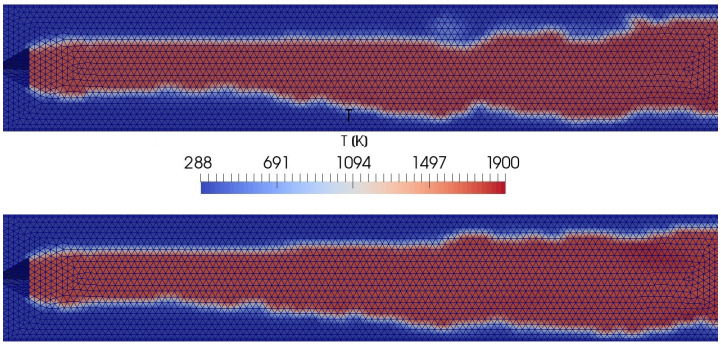

Figure 2.7: Instantaneous temperature maps for the case 1 with the PaSR model (top) and the LES-LEM baseline case (bottom) when using a very coarse tetrahedral mesh, cf. Tab. 2.1.

is similar to that using the PaSR model [114]. LES-LEM predictions with this mesh does not compare as well (with the experiments) as compared to the predictions done by using the hexahedral mesh. However, the goal here is to use a very coarse mesh, as often applied in engineering and industrial environments, to test the robustness of the current LES-LEM implementation.

2.3 Splicing investigation

Focus of this chapter is now shifted on treatment of a very important part of LES-LEM, i.e. treatment of large-scale advection via splicing. The dedicated investigation of the splicing is done without the complexity of chemically reacting flow physics, which makes it impossible to isolate and investigate the impact of the splicing on the global solution. Therefore, LES-LEM is qualitatively explored for turbulent passive scalar mixing.

The simulations of passive scalar transport in a co-flowing confined rectangular liquid jet are performed in OpenFOAM 2.0.x. Fig. 2.8 taken originally from [115] shows the test section of the jet. The Reynolds number is 20,000 and the inlet streams have velocities of 0.2, 0.4 and 0.2 m/s respectively. The passive scalar Rhodamine 6G was injected only in the middle stream while the outer two streams were pure water.

The computational domain is divided into 240, 90, 110 cells in x, y and z direction, respectively. The linear interpolation schemes and a second order least squares gradient scheme are used. The fixed walls are treated as no-slip and wall functions are used for the boundary layers. The exit uses

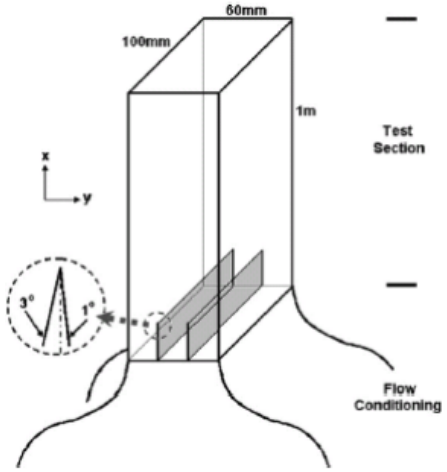

Figure 2.8: Schematics of jet test section [115]

a convective outflow boundary condition and zero gauge pressure. Zero-normal-gradient condition is used for pressure at the walls and the inflow boundary. For details see [98]

2.3.1 Comparisons with experiments

Fig. 2.9 shows plot of the instantaneous velocity at the middle z-normal plane.

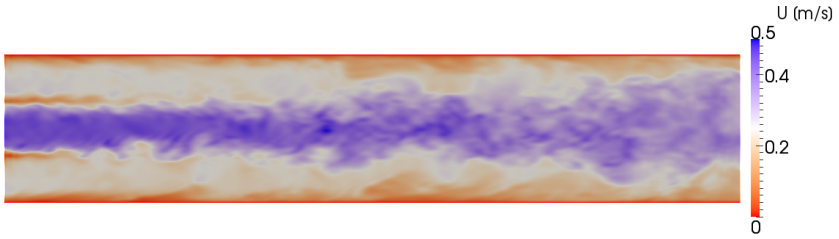

Figure 2.9: Instantaneous velocity contour plot in the middle z-normal plane at simulation time = 2.4 s

The results from the simulations were compared with the experiments at the middle z-normal plane at the same four downstream locations as done by Kong et al. [115], i.e. x/d = 1, 4.5, 7.5 and 12 (where d = 2cm). The simulations [98] predicted the velocity and passive scalar mixing statistics successfully.

Table 2.2: LES residence times at the four line locations.

Line locations	LES residence times/LES time step
x = 150 mm, y = 30 mm	30.3
x = 150 mm, y = 45 mm	48.8
x = 240 mm, y = 30 mm	32.6
x = 240 mm, y = 40 mm	39.7

2.3.2 Comparison of the new and old splicing strategy

The new splicing strategy should cause fluid residence times in a given LEM to agree more consistently with residence times on the LES side, which can be represented by $\Delta l/|\mathrm{u}|$. Here, Δl is a characteristic length scale of the LES cell and $|\mathrm{u}|$ is the LES cell velocity. To test this, the new splicing strategy was compared to previous approach by Menon and Kerstein [44]. Compared to the new approach, the approach of Menon and Kerstein [44] has the same order of attaching LEM segments to the input boundary, see Fig. 1.6 but the order of removal of LEM segments from the output boundary, see Fig. 1.5, is reversed, i.e. the highest-flux segments are removed before the lower-flux segments. Both strategies are compared here by looking at the PDF of residence times on the LEM domain. The construction of the PDF started from a statistically stationary solution. At the start of data gathering the residence time of each LEM cell was assigned to zero. After each LEM time advancement, the residence times were incremented equal to the advanced solution time. When a LEM cell is spliced out, its residence time was noted and set to zero for the spliced-in LEM cells. The residence times were collected for a total of 15500 LES time steps and PDF was constructed from the collected residence times.

The PDFs at four different line locations have been constructed as shown in Fig. 2.10. Y positions for the chosen lines were both in the middle of the domain (the left column in Fig. 2.10) and within the shear layer (the right column in Fig. 2.10). The PDFs in Fig. 2.10 show that the residence times fluctuate higher in the shear layer than in the middle of the domain which is an expected result as the highest velocity fluctuations are expected to be in the shear layer. By comparing the PDFs in Fig. 2.10 with Tab. 2.2, it is clear that the LEM residence times agree well with the residence times on the LES side.

Fig. 2.10 shows that there is a little difference between the PDFs of the new and the old splicing. This similarity can be explained here by the fact that in the current mixing test case, the splicing mass contribution in streamwise direction is much larger (and the dominant one) than in the

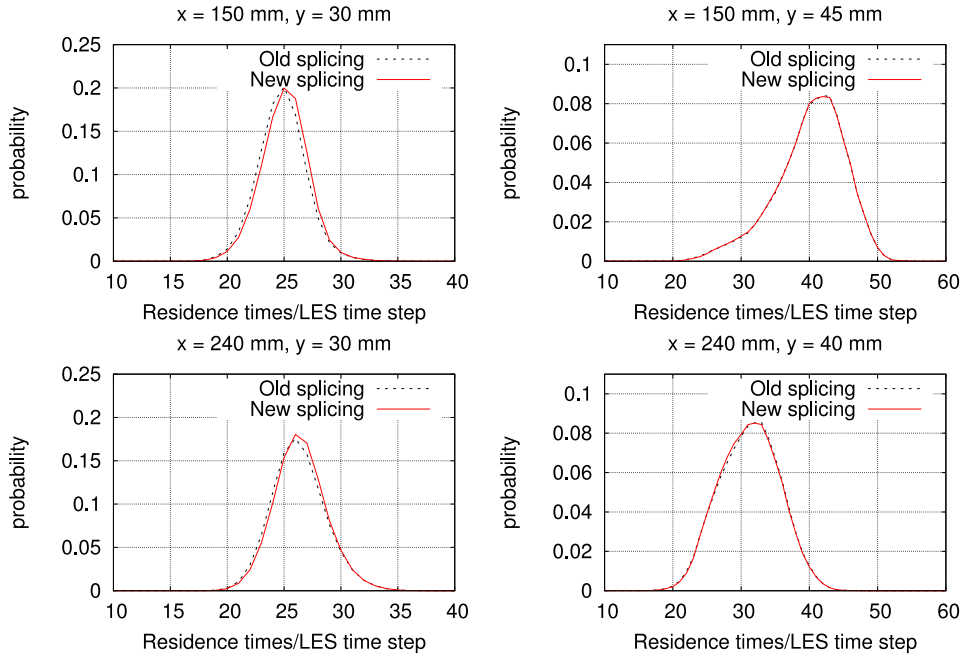

Figure 2.10: PDFs comparing residence time of spliced LEM segments for the new and the old splicing. The line x and y positions are shown in the title of each PDF.

two transverse directions. So whatever order the removal of LEM segments from the output boundary is, it does not influence the residence times much. However, for other mixing cases in which there is a comparable splicing mass contribution from all different directions, it is expected to have a bigger difference and therefore the new splicing strategy is expected to be better than the old one.

Conclusion

The main contributions of this thesis are:

- Implementation of LES-LEM in a pressure-based and unstructured grid solver in OpenFOAM.
- Development and implementation of a new LEM closure for LES with the reaction-rate approach. LES-LEM model with the new LEM closure was tested on the premixed Volvo combustor and the predictions were found to be within those of previous simulations.
- Development and implementation of a new splicing strategy based on an ordered flux of spliced LEM segments. The new splicing strategy was tested by simulating passive scalar mixing. The simulation results were compared to experiments and it was shown that the simulations correctly predict velocity statistics and passive scalar mixing. It was shown that the splicing represents large-scale advection in LES-LEM reasonably well, which has been implicitly assumed in combustion LES-LEM but never demonstrated in an isolated setting.
- Development and implementation of the super-grid LES-LEM. First demonstration of the expected computational speed-up compared to standard LES-LEM.

Future work

Although the tested case of the premixed Volvo combustor is challenging and showed similar results for LES-LEM and other, computationally more efficient models, it is not the type of problem where LES-LEM can demonstrate it's full potential which is mode and regime independence and a direct simulation of turbulence-chemistry interactions involving all scales. Future test cases for LES-LEM should focus on applications where these distinguished features of LES-LEM are relevant, e.g. low temperature combustion in engines and pollutant formation.

Super-grid LES-LEM

The LES-LEM combustion simulations are expensive because of having one LEM residing in each LES cell. To make LES-LEM less computationally expensive, a new LES-LEM modeling is proposed, called super-grid LES-LEM. In the super-grid LES-LEM, each LEM sits on a coarser mesh than the LES mesh called super-grid. Fig. 2 shows generation of the super-grid from the LES mesh. This concept of clustering LES cells in a super-grid cell results in reduced computational costs as compared to LES-LEM. The reason is that there are less number of LEM domains to advance the subgrid-scale LEM solution and also there are less number of splicing operations.

The super-grid LES-LEM does not lower the resolution on the LEM side, i.e. flame structures and turbulent flame chemistry interactions are still fully resolved. There is another modeling technique called the representative interactive LEM (RILEM) [116] in which there is one super-grid cell for all LES cells in the computational domain. Therefore, RILEM and LES-LEM are the two extremes and super-grid LES-LEM lies in between both of them.

During generation of the super-grid only coarsening (fusing together) of LES cells and LES mesh internal faces is done. There is no coarsening done on the LES mesh boundary. The super-grid exactly overlaps the LES mesh as shown in Fig. 2. Therefore, cell boundaries of the super-grid are faces of the LES mesh.

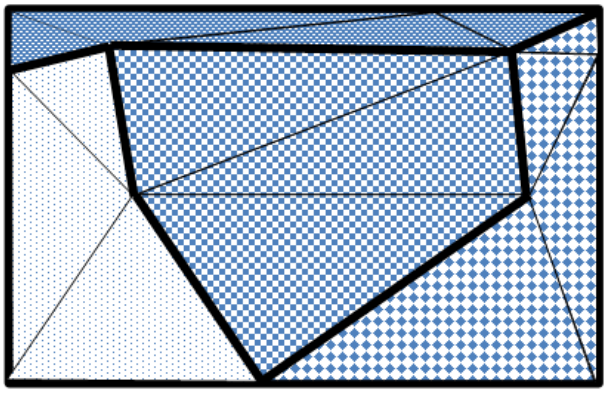

Figure 2: Super-grid generated from an unstructured LES mesh. LES mesh is shown by thin lines, whereas the generated super-grid (overlapping the thin lines of LES mesh) is shown by thick lines. In this figure, four super-grid cells (highlighted by a similar pattern) are generated from a total of fourteen LES cells.

Model formulation:

The super-grid is generated by using a geometric multigrid library from OpenFOAM extended 3.1. The library uses another library MGRIDGEN [117], which is based on METIS and contains various algorithms for generating a sequence of coarse meshes containing well-shaped cells. For the super-grid LES-LEM, only one level of coarser mesh is needed from the multigrid library. The LES mesh cells are fused together to form the super-grid cells based on a user input of minimum and maximum number of LES cells allowed to fuse together while having good quality super-grid cells. The super-grid quality becomes the objective function which is optimized by MGRIDGEN. See [118] for further details of the MGRIDGEN and [119] for the algorithms used by the MGRIDGEN.

The initial super-grid LEM line length is chosen to be equal to the local super-grid spacing. All the LEM cells in a super-grid cell are initialized uniformly with the thermochemical states in that super-grid cell. The thermochemical states in a super-grid cell are obtained by volume averaging the states in the corresponding LES cells (contained within that super-grid cell).

The chemical source terms obtained from a super-grid LEM domain are distributed equally to the LES cells (contained within that super-grid cell):

$$\bar{S}_{h,i} = S_{h,SG}/n,$$

$$\bar{S}_{\alpha,i} = S_{\alpha,SG}/n,$$

Table 1: Computational speed-up obtained by using the super-grid LES-LEM as compared to the LES-LEM. Left column of the table shows the user-input values for minimum and maximum number of LES cells allowed to fuse together to form a super-grid cell.

Super-grid coarsening parameters	Computational speed-up factor
min = 27, max = 30	12
min = 100, max = 125	25

where $S_{h,SG}$ and $S_{\alpha,SG}$ are the source terms obtained from a super-grid cell SG and n denotes the total number of LES cells contained within that super-grid cell. These LES source terms $\bar{S}_{h,i}$ and $\bar{S}_{\alpha,i}$ (for each LES cell i contained within that super-grid cell SG) are then used in the conservation equations for the species mass fractions and sensible enthalpy.

In the super-grid LES-LEM, splicing happens between individual LEM domains sitting on the super-grid. The splicing mass flux on a super-grid cell face is obtained by adding the mass fluxes on all the corresponding LES cell faces (which comprise that super-grid cell face).

Model validation:

The super-grid LES-LEM simulations were run on the Volvo test problem. The results are shown in Tab. 1, in which the comparison is done for advancing the subgrid-scale LEM solution. As shown in Tab. 1, the super-grid LES-LEM resulted in a high computational speed-up. However, the super-grid LES-LEM simulations resulted in an artificial extinction of the flame. The reason is that the current mapping of source terms from the super-grid LEM to the LES cannot capture the thin flame front structure in the premixed Volvo case.

A better strategy for coupling the super-grid LEM to the LES is proposed for future implementation, in which the super-grid LEM is coupled to the LES states using the RILEM [116] strategy. Namely, the LES time advances transport equations for mixture fraction mean and variance and for progress variable. The LES chemical states are then determined using the appropriate conditional averaging of LEM property profiles weighted by the assumed-shape joint PDF of the LES state variables. As shown in [116], this can provide the needed resolution of the types of features seen in the Volvo case.

Summary of papers

Paper 1

Effect of the turbulence modeling in large-eddy simulations of nonpremixed flames undergoing extinction and reignition

In this paper the effect of three turbulent combustion models, i.e. no-model, PaSR and LEM was studied for a flame with extinction and reignition. Two levels of mesh refinement and two eddy-viscosity models were used and two types of temporal jets were considered and their DNS results were qualitatively compared with LES results. It was found that LES captures qualitatively the extinction and reignition observed in the DNS simulations. The sensitivity to the turbulent combustion model was not negligible and the PaSR model showed the best accuracy. I implemented the LES-LEM model and ran the simulations together with Adhiraj Dasgupta. Esteban D. Gonzalez wrote the paper with support from me and Adhiraj Dasgupta who performed post-processing. Michael Oevermann provided supervision of the work.

Paper 2

Turbulent-combustion closure for the chemical source terms using the linear-eddy model

A new method to use LEM to close the filtered chemical source terms in the conservation equations of the thermochemical quantities is tested on a bluff-body stabilized flame case. The predictions using this closure were found to agree with experimental data within the same range of accuracy as the previous simulations. I implemented the new LEM closure for the LES-LEM model and improved the model from Paper 1 by further implementations. I assisted Esteban D. Gonzalez in the writing, by writing parts of the paper. Simulations were run by both me and Esteban D. Gonzalez.

This work was performed under guidance of Michael Oevermann and Suresh Menon.

Paper 3

A strategy for large-scale scalar advection in large eddy simulations that use the linear eddy sub-grid mixing model

A new strategy for splicing is implemented in a pressure-based fluid solver and tested by simulation of passive scalar transport in a co-flowing turbulent rectangular jet using unstructured grids. The simulation results showed good agreement with the experiments. This dedicated investigation of splicing concluded that the new splicing strategy represents large-scale advection in LES-LEM in a reasonable way. The new splicing strategy was proposed by Alan Kerstein and Michael Oevermann and Bo Kong provided the experimental data and simulation setup of the case. I implemented LES-LEM with the new splicing strategy, performed all the simulations, post-processed and analyzed the results. I wrote the paper with input from all the co-authors and presented it at the International Conference on Computational Heat and Mass Transfer held in Krakow in May 2016. The paper was chosen for publication as a Journal article in International Journal of Numerical Methods for Heat and Fluid Flow.

Paper 4

Subgrid reaction-diffusion closure for large eddy simulations using the linear-eddy model

In this paper a more detailed evaluation of the reaction-rate approach presented in paper 2 is done and more simulations were performed including a non-premixed syngas flame. After several months of simulating, post processing and analysis of the results I wrote this paper with input from all co-authors. The paper has been accepted for publication in Flow, Turbulence and Combustion.

References

[1] Kerstein, A.R.: Linear eddy modeling of turbulent transport and mixing. Combust. Sci. Technol. 60, 391-421 (1988)

[2] Peters, N.: Turbulent combustion. Cambridge Uni. Press (2000).

[3] Poinsot, T., Veynante, D.: Theoretical and Numerical Combustion. R. T. Edwards, Inc., Philadelphia (2005)

[4] Gonzalez-Juez, E.D., Kerstein, A.R., Ranjan, R., Menon, S.: Advances and challenges in modeling high-speed turbulent combustion in propulsion systems. Progr. Energy Combust. Sci. 60, 26-67 (2017)

[5] Oefelein, J.C.: Analysis of turbulent combustion modeling approaches for aero-propulsion applications. AIAA paper 2015-1378 (2015)

[6] Fureby, C.: A comparative study of large eddy simulation (LES) combustion models applied to the volvo validation rig. AIAA paper 2017-1575 (2017)

[7] Pitsch, H.: Large-Eddy simulation of turbulent combustion. Annual Review Fluid Mech. 38(4), 453-482 (2006)

[8] http://personalpages.to.infn.it/ fre/RTIgnitor/pdfversie/Petrosyan2.pdf

[9] Jhavar, R. and Rutland, C.J.: Using Large Eddy Simulations to Study Mixing Effects in Early Injection Diesel Engine Combustion. SAE Techn. Paper 2006-01-0871 (2006)

[10] Adomeit, P., Lang, O., Pischinger, S., Aymanns, R., Graf, M., Stapf, G.: Analysis of Cyclic Fluctuations of Charge Motion and Mixture Formation in a DISI Engine in Stratified Operation. SAE Techn. Paper 2007-01-1412 (2007)

[11] Yu, R., Bai, X.S., Hildingsson, L., Hultqvist, A., Miles, P.C.: Numerical and Experimental Investigation of Turbulent Flows in a Diesel Engine. SAE Techn. Paper 2006-01-3436 (2006)

[12] Yu, R., Bai, X.S., Vressner, A., Hultqvist, A., Johansson, B., Olofsson, J., Seyfried, H., Sjoholm, J., Richter, M., Alden, M.: Effect of Turbulence on HCCI Combustion. SAE Techn. Paper 2007-01-0183 (2007)

[13] Joelsson, T., Yu, R., Bai, X.S., Vressner, A., Johansson, B.: Large Eddy Simulation and Experiments of the Auto-Ignition Process of Lean Ethanol/Air Mixture in HCCI Engines. SAE Int. J. Fuels Lubricants 1(1), 1110-1119 (2008)

[14] Rutland, C. J.: Large-eddy simulations for internal combustion engines - a review. Int. J. Engine Res. 12(5), 421-451 (2011)

[15] Kösters, A., Golovitchev, V., Karlsson, A.: SAE, Int. J. Fuels Lubr., 5:604-610 (2012)

[16] Kösters, A., Karlsson, A., Oevermann, M., D'Errico, G., Lucchini, T.: Combust. Theory Model., 19:81-106 (2015)

[17] D'Errico, G., Lucchini, T., Contino, F., Jangi, M., Bai, X.S.: Combust. Theory Model., 18:65-88 (2014)

[18] Kong, S.C., Reitz, R.D.: J. Eng. Gas Turb. Power, 124:702-707 (2002)

[19] Kokjohn, S., Hanson, R.M., Splitter, D.A., Reitz, R.D.: SAE Technical Paper, 2009-01-2647 (2009)

[20] Knudsen, E., Kim, S.H., Pitsch, H.: Phys. Fluids, 22, 115109 (2010)

[21] Mittal, V., Pitsch, H.: Proc. Combust. Inst., 34:2995-3003 (2013)

[22] Peters, N.: Prog. Energy Combust. Sci., 10:319-339 (1984)

[23] Ihme, M., Pitsch, H.: Combust. Flame, 155:70-89 (2008)

[24] Nguyen, P., Vervisch, L., Subramanian, V., Domingo, P.: Combust. Flame, 157:43-61 (2010)

[25] Knudsen, E., Pitsch, H.: Combust. Flame, 159:242-264 (2012)

[26] Knudsen, E., Pitsch, H.: Combust. Flame, 156:678-696 (2009)

[27] Pitsch, H., Fedotov, S.: Combust. Theory, Model., 5:41-57 (2001)

[28] Pitsch, H., Cha, C.M., Fedotov, S.: Combust. Theory Model., 7:317-332 (2003)

[29] Lucchini, T., D'Errico, G., Onorati, A., Frassoldati, A., Stagni, A., Hardy, G.: SAE Int. J. Engines, 10:2017 (2017)

[30] Barths, H., Hasse, C., Bikas, G., Peters, N.: Proc. Combust. Inst., 28:1161-1168 (2000)

[31] Barths, H., Antoni, C., Peters, N.: SAE Technical Paper, 982459 (1998)

[32] Hasse, C., Barths, H., Peters, N.: SAE Technical Paper, 1999-01-3547 (1999)

[33] Hergarth, C., Barths, H., Peters, N.: SAE Technical Paper, 1999-01-3550 (1999)

[34] Pitsch, H., Wan, H., Peters, N.: SAE Technical Paper, 952357 (1995)

[35] Pitsch, H., Barths, H., Peters, N.: SAE Technical Paper, 962057 (1996)

[36] Maghbouli, A., Lucchini, T., D'Errico, G., Onorati, A., Malbec, L. M., Musculus, M., Eagle, W.E.: SAE Technical Paper, 2016-01-0577 (2016)

[37] Klimenko, A.Y., Bilger, R.W.: Prog. Energy Combust. Sci., 25:595-688 (1999)

[38] Paola, G. De, Mastorakos, E., Wright, Y. M., Boulouchos, K.: Comb. Sci. Tech., 180:883-899 (2008)

[39] Bolla, M., Farrace, D., Wright, Y.M., Boulouchos, K.: Fuel, 117:309-325 (2014)

[40] Pope, S.B.: Annu. Rev. Fluid, Mech., 26:23-63 (1994)

[41] Zhang, Y.Z., Kung, E.H., Haworth, D.C.: Proc. Combust. Inst., 30:2763-2771 (2005)

[42] Mohan, V.R., Haworth, D.C.: Proc. Combust. Inst., 3053-3060 (2015)

[43] Menon, S., Kerstein, A.R., McMurtry, P.A.: A linear eddy mixing model for large eddy simulation of turbulent combustion. In: Large Eddy Simul. Complex Eng. Geophysical Flows, Galperin, B., Orszag, S.A., pp. 287-314. Cambridge University Press (1993)

[44] Menon, S., Kerstein, A.R.: The Linear-Eddy Model. In: Turbulent Combustion Modeling, Echekki, T., Mastorakos, E., pp. 221-247. Springer Series, Vol. 95, New York (2011)

[45] Kerstein, A.R.: Linear-eddy modelling of turbulent transport. Part 7. Finite-rate chemistry and multi-stream mixing. J. Fluid Mech. 240, 289-313 (1992)

[46] Menon, S., Sankaran, V., Stone, C.: Subgrid combustion modeling for the next generation National Combustion Code. NASA Tech. Rep. 2003-212202 (2003)

[47] Sankaran, V.: Subgrid combustion modeling for compressible two-phase reacting flow. Ph.D. thesis, Georgia Institute of Technology (2003)

[48] Porumbel, I., Menon, S.: Large eddy simulation of bluff body stabilized premixed flame. AIAA Paper 2006-152 (2006)

[49] Parisi, V.: Large Eddy Simulation of a Non-Premixed Stagnation Point Reverse Flow Combustor. Master's thesis, Georgia Institute of Technology (2006)

[50] Undapalli, S.: Large eddy simulation of premixed and non-premixed combustion in a stagnation point reverse flow combustor. Ph.D. thesis, Georgia Institute of Technology (2008)

[51] Sen, B.A., Menon, S.: Artificial neural networks based chemistry-mixing subgrid model for LES. AIAA Paper 2009-241 (2009)

[52] Genin, F., Menon, S.: Simulation of turbulent mixing behind a strut injector in supersonic flow. AIAA Paper 2009-132 (2009)

[53] Wey, T., Liu, N.: Assessment of turbulence-chemistry interaction models in the National Combustion Code (NCC) - Part I. AIAA Paper 2010-16098 (2010)

[54] Liu, N., Wey, T.: On the TFNS Subgrid Models for Liquid-Fueled Turbulent Combustion. AIAA Paper 2014-3569 (2014)

[55] Harvazinski, M.E., Huang, C., Sankaran, V., Feldman, T.W., Anderson, W.E., Merkle, C.L., Talley, D.G.: Coupling between hydrodynamics, acoustics, and heat release in a self-excited unstable combustor. Phys. Fluids 27, No. 4, 045102 (2015)

[56] Fureby, C., Zettervall, N., Kim, S., Menon, S.: Large eddy simulation of a simplified lean premixed gas turbine combustor. Intl. Symp. Turbul. Shear Flow Phenom. (2015)

[57] Maxwell, B.M., Falle, S.A.E.G., Sharpe, G., Radulescu, M.I.: A compressible-LEM turbulent combustion subgrid model for assessing gaseous explosion hazards. J. Loss Prevention Process Industries 36, 460-470 (2015)

[58] Li, S., Zheng, Y., Mira, D., Li, S., Zhu, M., Jiang, X.: A LES-LEM study of preferential diffusion processes in a partially premixed swirling combustor with synthesis gases. J. Eng. Gas Turbine Power 139, 031501 (2016)

[59] McMurtry, P.A., Menon, S., Kerstein, A.R.: A linear eddy sub-grid model for turbulent reacting flows: Application to hydrogen-AIR combustion. Proc. Combust. Inst. 24, 271-278 (1992)

[60] Calhoon, W.H.: On subgrid combustion modeling for large-eddy simulations. PhD thesis, Georgia Institute of Technology (1996)

[61] Menon, S., Calhoon, W.H.: Subgrid mixing and molecular transport modeling in a reacting shear layer. Proc. Combust. Inst. 26, 59-66, (1996)

[62] Smith, T.M.: Unsteady simulations of turbulent premixed reacting flows. PhD thesis, Georgia Institute of Technology (1998)

[63] Chakravarthy, V.K., Menon, S.: Subgrid modeling of turbulent premixed flames in the flamelet regime. Flow, Turbul. Combust. 65, 133-161 (2000)

[64] Pannala, S., Menon, S.: Large eddy simulations of two-phase turbulent flows. AIAA Paper 1998-0163 (1998)

[65] Zimberg, M.J., Frankel, S.H., Gore, J.P., Sivathanu, Y.R.: A study of coupled turbulent mixing, soot chemistry, and radiation effects using the linear eddy model. Combust. Flame 113, 454-469 (1998)

[66] Sankaran, V., Menon, S.: Subgrid combustion modeling of 3-D premixed flames in the thin-reaction-zone regime. Proc. Combust. Inst. 30, 575-582 (2005)

[67] Sen, B.A., Menon, S.: Linear eddy mixing based tabulation and artificial neural networks for large eddy simulations of turbulent flames. Combust. Flame 157, 62-74 (2010)

[68] Sen, B.A., Hawkes, E.R., Menon, S.: Large eddy simulation of extinction and reignition with artificial neural networks based chemical kinetics. Combust. Flame 157, 566-578 (2010)

[69] Ochoa, J.S., Sanchez-Insa, A., Fueyo, N.: Subgrid linear eddy mixing and combustion modelling of a turbulent nonpremixed piloted jet flame. Flow, Turbul. Combust. 89, 295-309 (2012)

[70] Choi, J.J., Menon, S.: Large eddy simulation of cavity-stabilized supersonic combustion. AIAA Paper 2009-5383 (2009)

[71] Sone, K., Menon, S.: Effect of subgrid modeling on the in-cylinder unsteady mixing process in a direct injection engine. J. Eng. Gas Turbines Power 125(2), 435-443 (2003)

[72] Steeper, R., Sankaran, V., Oefelein, J., Hessel, R.: Simulation of the effect of spatial fuel distribution using a linear-eddy model. SAE Technical Paper 2007-01-4131 (2007)

[73] Martinez, D.M., Jiang, X., Moulinec, C., Emerson, D.R.: Numerical simulations of turbulent jet flames with non-premixed combustion of hydrogen-enriched fuels. Comput. & Fluids 88, 688-701 (2013)

[74] Martinez, D.M., Jiang, X., Moulinec, C., Emerson, D.R.: Numerical assessment of subgrid scale models for scalar transport in large-eddy simulations of hydrogen-enriched fuels. Int. J. Hydrogen Energy 39, 7173-7189 (2014)

[75] Lovett, J.A., Ahmed, K., Bibik, O., Smith, A.G., Lubarsky, E., Menon, S., Zinn, B.T.: On the influence of fuel distribution on the flame structure of bluff-body stabilized flames. J. Eng. Gas Turbines Power 136(4), 041503 (2013)

[76] Srinivasan, S., Ranjan, R., Menon, S.: Flame dynamics during combustion instability in a high-pressure, shear-coaxial injector combustor. Flow, Turbul. Combust. 94, 237-262 (2015)

[77] Srinivasan, S., Kozaka, E.O., Menon, S.: A new subgrid breakup model for LES of spray mixing and combustion. In: Direct and Large-Eddy Simulation VIII, pp. 333-338. ERCOFTAC, Springer Science and Business Media (2011)

[78] Pope, S.B.: PDF methods for turbulent reactive flows. Prog. Energy Combust. Sci. 11, No. 2, 119-192 (1985)

[79] Haworth, D.C.: Progress in probability density function methods for turbulent reacting flows. Prog. Energy Combust. Sci. 36, No. 2, 168-259 (2010)

[80] Haworth, D.C., Pope, S.B.: Transported probability density function methods for Reynolds-averaged and large-eddy simulations. Turbulent Combust. Model., 119-142 (2011)

[81] Pope, S.B.: Small scales, many species and the manifold challenges of turbulent combustion. Proc. Combust. Inst. 34, No. 1, 1-31 (2013)

[82] Wu, H., See, Y.C., Wang, Q., Ihme, M.: A pareto-efficient combustion framework with submodel assignment for predicting complex flame configurations. Combust. Flame 162, No. 11, 4208-4230 (2015)

[83] Gada, V.H., Tandon, M.P., Elias, J., Vikulov, R., Lo, S.: A large scale interface multi-fluid model for simulating multiphase flows. Appl. Math. Model. 44, 189-204 (2017)

[84] OpenFOAM, software available at http://www.openfoam.org.

[85] Weller, H.G., Tabor, G., Jasak, H., Fureby, C.: A tensorial approach to computational continuum mechanics using object-oriented techniques. Comput. Phys. 12, No. 6, 620-631 (1998)

[86] Yoshizawa, A., Horiuti, K.: A statistically-derived subgrid-scale kinetic energy model for the large eddy simulation of turbulent flows. J. Phys. Soc. Japan 54, 2834-2839 (1985)

[87] Gonzalez-Juez, E.D., Dasgupta, A., Arshad, S., Oevermann, M., Lignell, D.: Effect of the turbulence modeling in large-eddy simulations of nonpremixed flames undergoing extinction and reignition. AIAA Paper 2017-0604 (2017)

[88] Kerstein, A.R.: One-dimensional turbulence: model formulation and application to homogeneous turbulence, shear flows, and buoyant stratified flows. J. Fluid Mech. 392, 277-334 (1999)

[89] Grøvdal, F.: A dimensional-decomposition approach for stochastic scale-resolving simulations of turbulent reacting flows. Ph.D. thesis, Norwegian University of Science and Technology (2018)

[90] Richardson, L.F.: Weather Prediction by Numerical Process. Republication. Dover Publ., New York 1965. (Cambridge Univ. Press, London) (1922)

[91] Richardson, L.F.: Atmospheric diffusion shown on a distance-neighbour graph. Proceedings of the Royal Society of London. Series A, Containing Papers of a Mathematical and Physical Character, 110(756):709-737 (1926)

[92] Issa, R.I.: Solution of the implicitly discretised fluid flow equations by operator-splitting. J. Comput. Phys. 62, No. 1, 40-65 (1986)

[93] Arshad, S., Gonzalez-Juez, E.D., Dasgupta, A., Menon, S., Oevermann, M.: Subgrid reaction-diffusion closure for large eddy simulations using the linear-eddy model. Flow, Turbul. Combust. submitted (2018)

[94] Sjunnesson, A., Nelson, C., Max, E.: LDA Measurements of velocities and turbulence in a bluff body stabilized flame. Proc. 4th Intl. Conf. Laser Anemometry, Cleveland, OH (1991)

[95] Sjunnesson, A., Olovsson, S., Sjoblom, B.: Validation rig – A tool for flame studies. Volvo Flygmotor Intern. Rep. VFA 9370-308 (1991)

[96] Sjunnesson, A., Henrikson, P., Lofstrom, C.: CARS measurements and visualization of reacting flows in a bluff body stabilized flame. AIAA Paper 1992-3650 (1992)

[97] Ma, F., Proscia, W., Ivanov, V., Montanari, F.: Large eddy simulation of self-excited combustion dynamics in a bluff-body combustor. AIAA Paper 2015-3968 (2015)

[98] Arshad, S., Kong, B., Kerstein, A.R., Oevermann, M.: A strategy for large-scale scalar advection in large eddy simulations that use the linear eddy sub-grid mixing model. Intl. J. Numer. Methods Heat Fluid Flow, in press (2018)

[99] Duwig, C., Nogenmyr, K., Chan, C., Dunn, M.J.: Large eddy simulations of a piloted lean premix jet flame using finite-rate chemistry. Combust. Theory Model. 15, No. 4, 537-568 (2011)

[100] Fiorina, B., Mercier, R., Kuenne, G., Ketelheun, A., Avdić, A., Janicka, J., Geyer, D., Dreizler, A., Alenius, E., Duwig et al. C.: Challenging modeling strategies for LES of non-adiabatic turbulent stratified combustion. Combust. Flame 162, No. 11, 4264-4282 (2015)

[101] Möller, S., Lundgren, E., Fureby, C.: Large eddy simulation of unsteady combustion. Int. Symposium Combust. 26, No. 1, 241-248 (1996)

[102] Fureby, C.: Large eddy simulation of combustion instabilities in a jet engine afterburner model. Combust. Sci. Technol. 161, No.1, 213-243 (2000)

[103] Comer, A.L., Huang, C., Rankin, B.A., Harvazinski, M.E., Sankaran, V.: Modeling and simulation of bluff body stabilized turbulent premixed flames. AIAA Paper 2016-1936 (2016)

[104] Giacomazzi, E., Battaglia, V., Bruno, C.: The coupling of turbulence and chemistry in a premixed bluff-body flame as studied by LES. Combust. Flame 138, No. 4, 320-335 (2004)

[105] Cocks, P.A.T., Soteriou, M.C., Sankaran, V.: Impact of numerics on the predictive capabilities of reacting flow LES. Combust. Flame 162, No. 9, 3394-3411 (2015)

[106] Baudoin, E., Nogenmyr, K.J., Bai, X.S., Fureby, C.: Comparison of LES models applied to a bluff body stabilized flame. AIAA Paper 2009-1178 (2009)

[107] Fureby, C.: A comparative study of large eddy simulation (LES) combustion models applied to the Volvo validation rig. AIAA Paper 2017-1575 (2017)

[108] Drennan, S.A., Kumar, G., Liu, S.: Developing grid-convergent LES simulations of augmentor combustion with automatic meshing and adaptive mesh refinement. AIAA Paper 2017-1574 (2017)

[109] Gonzalez-Juez, E.D.: Numerical simulations of thermoacoustic combustion instabilities in the Volvo combustor. AIAA Paper 2017-4686 (2017)

[110] Wu, H., Ma, P.C., Lv, Y., Ihme, M.: MVP-workshop contribution: Modeling of Volvo bluff body flame experiment. AIAA Paper 2017-1573 (2017)

[111] Sankaran, V., Gallagher, T.: Grid convergence in LES of bluff body stabilized flames. AIAA Paper 2017-1791 (2017)

[112] Durand, L., Polifke, W.: Implementation of the thickened flame model for large eddy simulation of turbulent premixed combustion in a commercial solver. ASME Paper GT2007-281888 (2007)

[113] Jones, W.P., Marquis, A.J., Wang, F.: Large eddy simulation of a premixed propane turbulent bluff body flame using the Eulerian stochastic field method. Fuel 140, 514-525 (2015)

[114] Nordin, P.A.N.: Complex chemistry modeling of diesel spray combustion. Ph.D. thesis, Chalmers University of Technology (2001)

[115] Kong, B., Olsen, M. G., Fox, R. O., Hill, J. C.: Predictive capability of Large Eddy Simulation for point-wise and spatial turbulence statistics in a confined rectangular jet. Chem. Engineering Sci. 69, 240-256 (2012)

[116] Lackmann, T.: A representative interactive linear-eddy-model (RILEM) for simulating spray combustion. Ph.D. thesis, Chalmers University of Technology (2017)

[117] Available at http://www-users.cs.umn.edu/ moulitsa/software.html

[118] Available at http://www-users.cs.umn.edu/ moulitsa/download/manual-parmgridgen.pdf

[119] Moulitsas, I., Karypis, G.: Multilevel algorithms for generating coarse grids for multigrid methods. Supercomputing Conf. Proc. (2001)